2013

Analytical and field investigation of horizontally curved girder bridges

Jerad James Hoffman
Iowa State University

Analytical and field investigation of horizontally curved girder bridges

by

Jerad J. Hoffman

A thesis submitted to the graduate faculty

in partial fulfillment of requirements for the degree of

MASTER OF SCIENCE

Major: Civil Engineering (Structural Engineering)

Program of Study Committee:
Brent M. Phares, Co-major Professor
Terry J. Wipf, Co-major Professor
Loren W. Zachary

Iowa State University

Ames, Iowa

2013

TABLE OF CONTENTS

v

LIST OF FIGURES

LIST OF TABLES

LIST OF VARIABLES

A_c = the area of concrete

A_s = the area of the steel

B_e = effective slab width,

D = the depth of the web

DAF = dynamic amplification factor

DC = dead load for structural components

$(EA)_{eff}$, = effective axial rigidity

E_c = the linear elastic modulus of concrete

E_s = the linear elastic modulus of steel

I_f = moment of inertia of a flange about its smaller principal axis

I_{ytb}(steel) = moment of inertia of the bottom flange for Y-axis bending

I_{ytf}(steel) = moment of inertia of the top flange for Y-axis bending

IM = dynamic impact factor for live load

L = length of bridge along curve

L_e = equivalent cantilever length

LL = vehicular live load

M_{lb} = lateral bending moment in the bottom flange

M_{lt} = lateral bending moment in the top flange

M_x = strong axis bending moment

MDF = moment distribution factors

N = V-Load equation constant of either 10 or 12 (engineer's discretion)

P = the internal axial force

TG	= force effect due to temperature gradient
TU	= force effect due to uniform temperature
Y(NA)	= the distance to the neutral axis measured from the center of the bottom flange
d	= centerline concrete slab to centerline bottom flange
t_s	= slab thickness
x	= distance from center of flange to flange tip
x_i	= distance from neutral axis to strain gauge i along the X-axis
y_i	= distance from neutral axis to strain gauge i along the Y-axis
$\bar{y}$	= distance from the center of the bottom flange to the neutral axis
α_c	= the thermal expansion of concrete
α_s	= the thermal expansion of steel
ε_a	= internal axial strain
ε_{ylt}	= lateral bending strain in the top flange
ε_{ylb}	= lateral bending strain in the bottom flange
ε_i	= strain reading at gauge i
ε_x	= strong axis bending strain
ΔT_{eff}	= the effective bridge temperature
ΔT_c	= the change in temperature of the concrete member
ΔT_s	= the change in temperature of the steel member
σ_x	= strong axis bending stress (ksi)
σ_{lb}	= lateral bending stress in the bottom flange (ksi)
σ_a	= axial stress (ksi)
γ_P	= design load factor for permanent loads

γ_{TG} = design load factor for temperature gradients

γ_{TU} = design load factor for uniform temperature

ABSTRACT

Nationally, concerns have been raised regarding the relatively new design approach of combining the use of integral abutments with horizontally curved steel I-girder bridges. In order to address concerns regarding the superstructure behavior, this research experimentally and analytically investigated four in-service, horizontally curved, steel I-girder bridges with integral and semi-integral abutments. These bridges are located at the major interchange of Interstates I-235 and I-80. For the research, a monitoring system was installed on the bridges using an array of strain gauges. The implications of the critical data that the monitoring system produced will enable further development of design specifications for similar bridge types, particularly with respect to thermal effects. In addition to the measured field data, an analytical model for one of the instrumented bridges was established using a commercial finite element analysis software package. Several conclusions were formed from both of the experimental and analytical results. First, the short term experimental results produced moment distribution factors that were most heavily influenced by the degree of curvature. Also from the short term results, a simplified analysis method, referred to as the V-Load method, provided only an approximate preliminary assessment of the lateral bottom flange bending based on the degree of curvature with minimal skew. Next, the long term experimental results indicated that an effective thermal range of 100^0F may cause up to 12 ksi of additional stress in the girders due to restrained expansion and contraction of the bridge. Lastly, results from the analytical investigation indicated that the stresses in the lower flange of the girder, due to applied thermal loads, were greatest at the fixed pier locations. These stresses were mostly due to lateral flange bending caused by the fixed pier restraining lateral movement of the curved girder. Based on the experimental and analytical investigations, the findings within this research suggest that similar bridges require a refined method of analysis when incorporating integral abutments and fixed piers. More importantly, bridges with increased curvature and skew may require special attention in future practice as lateral bending stresses may increase due to temperature loads.

ACKNOWLEDGEMENTS

CHAPTER 1 GENERAL INTRODUCTION

The contents of this thesis report include a collection of research that has been prepared for submission to scholarly journals. Both of the modified journal papers, presented in subsequent chapters, address the growing interests and concerns of horizontally curved steel I-girder bridges with integral abutments. This chapter introduces the journals by discussing the industry problems, research scope and objectives, and organization of the thesis.

1.1 Industry Problem

Around 25% of the Nation's steel girder bridges are designed with horizontal curvature. Of these bridges, growing amounts are including integral abutments in their design due to their desirable characteristics. Since these bridges are rather new to the Nation, designers are somewhat unfamiliar with certain effects of using integral with horizontal curvature. Incorporating horizontal curvature with integral abutments in steel girder bridges raises issues concerning structure behaviors. However, a great need exists to reduce maintenance costs in bridges by reducing the number of deck joints. The installation and maintenance of bearing joints can be problematic due to leaky joints which result in corrosion and buildup of debris at the bearings. Solving these costly maintenance issues can be accomplished by advancing the use of integral abutments. Because of their efficiency, the need for integral abutments in curved bridges is on the rise. Consequently, the National Cooperative Highway Research Program has decided that funding future research regarding the design and construction of curved steel girder bridges is of high importance.

1.2 Objectives and Scope of the Research

The purpose of this research was to explore horizontally curved steel I-girder bridges with integral abutments through field evaluations and analytical investigations. In 2008, the Iowa Department of Transportation started the re-construction of the intersection of Interstates I-35, I-80 and, I-235 (Northeast Mix-Master) that included six new bridges. The development of the Northeast Mix-Master (NEMM) provided the opportunity for a research team to evaluate and assess the behavior of curved-steel I-girder bridges as the new bridges were designed with varying curvature, skew, and support conditions. These evaluations and assessments incorporated instrumentation that accounted for both long term and short term

behaviors of the bridges. The research team, consisting of professors and students at Iowa State University (ISU) in combination with members of the Iowa Department of Transportation (DOT), narrowed the focus of the long and short term behaviors to thermal loads and live loads. To fully address the behaviors of these bridges, influences of the different support conditions with varying degrees of skew were considered throughout the research. As a result of the study, general observations and conclusions were noted throughout to potentially pose recommendations for future design and research practices on these types of bridges.

1.3 Organization of the Document

Chapter 1 of this document introduces the research, the background, the objectives and scope, and the overall organization of the contents. Chapter 2 discusses a review of past literature and research performed on similar bridges. Chapter 3 discusses the live load field testing procedures that produced the results in Chapters 4 and 5.

Chapter 4 presents a scholarly journal paper that has been prepared for submission to the *Transportation Research Record: Journal of the Transportation Research Board.* The subjects include long and short term health monitoring along with field evaluations of both horizontally curved and straight girder bridges located at the NEMM. The work presented in Chapter 4, with respect to the long term research, are results formulated in the previously written thesis, *Field Monitoring and Evaluation of Curved Girder Bridges with Integral Abutments* by Shryack et al. (2012) at Iowa State University. Results from the thesis were made available to supplement the short term assessments and further analytical investigations. All research regarding the NEMM bridges was performed by the Iowa State University Bridge Engineering Center as part of a pooled fund study sponsored by the Iowa DOT.

Chapter 5 presents a scholarly journal paper that has been prepared for submission to ASCE's *Journal of Bridge Engineering.* The contents include an analytical investigation for design loading conditions on a single horizontally curved steel girder bridge. The bridge of focus was previously subjected to the field monitoring mentioned in Chapter 4. Field results from Chapter 4 provided a prime opportunity to further investigate, validate, and compare analytical results to measured field results.

3

Lastly, Chapter 6 summarizes general observations and conclusions from the journal paper results. Possible recommendations for future research focused on horizontally curved bridges were suggested accordingly. Note that Chapters 4 and 5 contain brief summaries of the content discussed in Chapters 1 through 3. The brief summaries provide essential information for the journal papers as Chapters 1 through 3 will not be readily available to the reader of the two journal papers.

The three authors listed in the two journal papers were part of the NEMM research team at the ISU Bridge Engineering Center. Gus Shryack and Jerad Hoffman were graduate research assistants under the supervision of Dr. Brent Phares, P.E., Dr. Terry Wipf, P.E., and Dr. Lowell Greimann, P.E. Gus Shryack contributed to the long term field monitoring research and Jerad Hoffman contributed to the short term field monitoring and analytical modeling research.

CHAPTER 2 LITERATURE REVIEW

The contents of this chapter attempt to summarize and review the rather limited amount of completed work on horizontally-curved, integral-abutment bridges. In doing so, the behavior, mechanics, and analysis of horizontally curved steel girders will be discussed throughout.

2.1 Mechanics and Behavior of Horizontally Curved Girders

Miller et al. (2009) state that curved beams create twisting effects which result in warping out of plane similar to torsion. This phenomenon is referred to as a bimoment, a product of combined bending and torsional shear. In addition, negligible secondary effects occur when the curved compression flange bows outwards, increasing the degree of curvature. When secondary effects are introduced, lateral bending in the flange results in a variation of bending stresses across the flange width.

Lydzinski et al. (2008) further explain additional complications that arise when analyzing and designing I-girders in curved bridges. Complications range from the individual plates to the constructed girder as a whole. Compared to straight girders, horizontally-curved I-girders are significantly different in the following ways:

- Flange local buckling may differ from the outer to the inner side of the web.
- Local buckling is possible on the inner half of the tension flange.
- S-shaped bending occurs in the web, causing an increase of stress at the web-flange connection.
- Bending and torsion stresses are not decoupled, resulting in lateral bending behavior.
- Twisting can occur under individual girder self-weight, causing construction issues in framing.

In NCHRP Report 424, Hall et al. (1999) describe that vertical bending is broken down into the first three components shown in Figure 2.1. Components 3 and 4 pertain to curved girders while Components 1 and 2 are also present in straight girders. Component 1 consists of a load applied directly through the shear center of the girder. Component 2 is the restoring moment from cross frames or diaphragms connecting to adjacent girders. Forces in connecting members are created due equilibrium effects. Component 3 is due to the

horizontal curvature of the girder. Lastly, lateral flange bending is represented in Component 4. Component 4 causes longitudinal stress in the girder flanges due to nonuniform torsion shown in Figure 2.2. Lateral flange bending can be divided into warping stresses, radial bending, and second order effects. Radial forces are created due to cross frames, while axial forces result from vertical bending in the curved member. An approximation of lateral flange bending can be addressed through the well-known V-load equation, discussed subsequently.
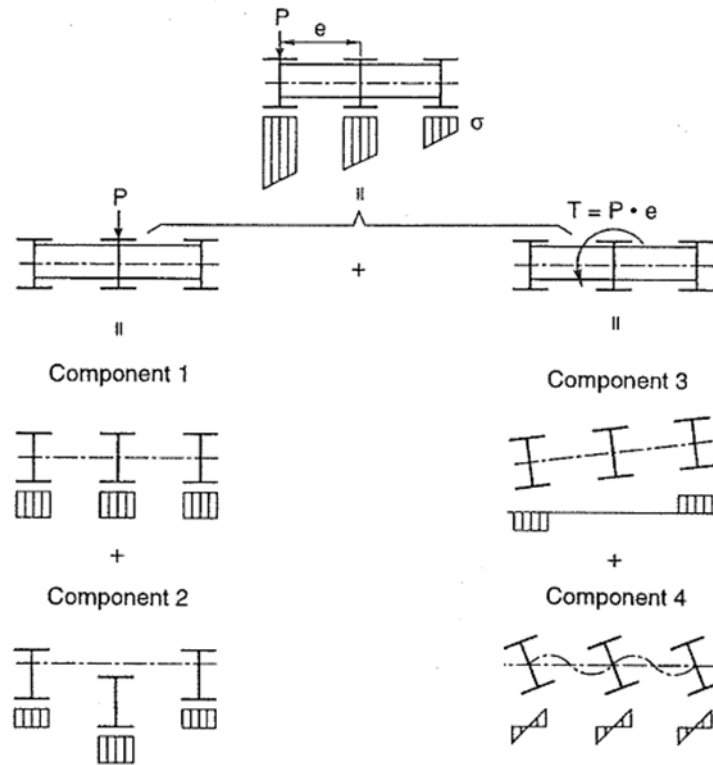
Figure 2.1. Four normal stress components from Figure A-5. Hall et al. (1999)
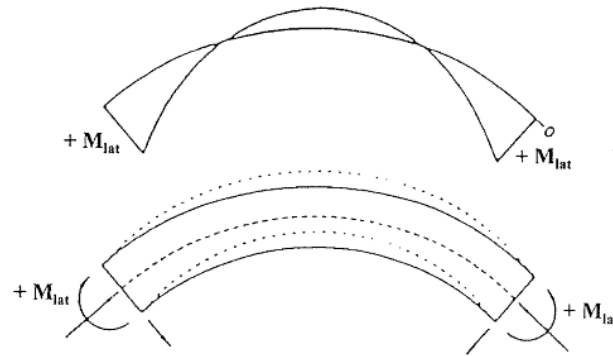
Figure 2.2. Lateral Flange Bending Diagram from Figure A-1. Hall et al. (1999)

Several levels of analysis can be used to determine girder responses. These include, but are not limited to, the line girder method, grid method, finite strip method, and finite element modeling (FEM) analysis method. The simplest technique, line-girder method, assumes only vertical loads applied to a single girder. Engineers must determine the amount of load and location of load between girders. Component 1 is only considered during the line-girder analysis and Component 3 may be considered if the V-load method is also applied. The grid analysis considers Components 1, 2, and 3. Warping torsion is not recognized in the grid analysis, since only St. Venant torsion is used. Again, applying the V-load method indirectly accounts for lateral flange bending. Finite element analysis is capable of determining Components 1, 2, and 3. If large-deflection theory is used, then the effects of warping stress may also be accounted for (Hall et al. 1999).

2.2 Comparing Levels of Analysis for Horizontally Curved Bridges

Very few studies have thoroughly compared different methods of analysis with respect to field test results in horizontally curved bridges. Nevling et al. (2006) attempt to evaluate the level of accuracy produced for various analysis methods through conducting research on a continuous three-span bridge. Table 2.1 details the three levels of analysis performed in the study. The bridge of interest is constructed of five, Grade 50, steel plate I-girders with the outside girder having a radius of 178.5 m (585.6 ft). The non-integral abutment skews range from 60^0 to 35^0.

An American Association of State Highway and Transportation Officials (AASHTO) HS20 design truck was applied as a live load to the bridge at various locations. The single

instrumented radial cross-section focused on in this paper, includes the location of maximum positive moment at center span. At this location, strain gauges were placed on the four flanges on each of the five girders to analyze the superstructure's reaction to live loading.

Table 2.1. Levels of Analysis from Table 1 Nevling et al. (2006)

Level	Description	Analysis Tool
1	Manual	AASHTO Guide Specs
		V-load Method
2	2D Grillage	SAP2000
		MDX
		DESCUS
3	3D FEM	SAP2000
		BSDI

The study made conclusions comparing the three methods of analysis against one another, as well as the methods against field data. Compared to field results, Level 1 analyses predicted larger major axis bending moments for girders closer to the applied load and smaller major axis bending moments for girders furthest from the applied load. Correlations between Level 1 and 3 analyses to field results were inconclusive with respect to lateral bottom flange bending moments. Levels 2 and 3 predicted major axis bending moments similar to the field results. However, Level 2 predicted more accurate vertical bending moments compared to Level 1. The study concluded that Level 3 did not provide increased accuracy that was noticeable compared to Level 2 analyses. Thus, Level 2 analysis would be recommended based on the study's findings.

Miller et al. (2009) also conducted a study comparing field testing to FEM. The study focused on a multi-girder, three-span, steel composite, horizontally curved I-girder bridge. Field testing consisted of attaching several strain gauges to the steel girders and diaphragms. Static and dynamic loading, similar to an HS20 truck, was applied and later replicated on a FEM. Results concluded that the FEM predicted a higher neutral axis location compared to the field results and composite section theory. The cause may be due to slippage of the shear studs in the haunches.

Field data analysis further concluded that web lateral bending is present. Also, the neutral axis of the composite section was located below the top flange of the girder. Comparing the FEM to field results showed that larger diaphragm shear strains were found in the field than provided by FEM analysis. In addition, including pier flexibility most accurately compared to the field results. Lastly, a correlated straight girder analysis yielded the neutral axis below the top flange, indicating that the curved girder may require a refined mesh in the FEM to simulate for the complex strain distribution (Miller et al. 2009).

Another FEM study was performed by Lydzinski et al. (2008). The FEM replicated a continuous three-span horizontally curved I-girder bridge comparing dynamic and static loading responses. Dynamic loading concentrated on free vibrations. FEM found that plate elements adequately represented plate bending behavior and interactions in the cross framing. Refined meshing is more critical along the longitudinal direction of the bridge versus the transverse direction at a particular cross-section. Modeling the haunch with plate elements provided negligible differences compared to using rigid links. The authors further found that the piers can be modeled using beam elements rather than complicated 3D elements. Finally, the overall conclusion of the study indicated that including the pier model flexibility is significant in estimating the behavior of the entire bridge.

Barr et al. (2007) investigated the live-load response of a three span horizontally curved I-girder bridge. The study pertains to comparing field test data to a FEM analysis, as well as the V-load method. Conclusions of the study offer suggestions regarding FEM analysis results. These suggestions explore differences between the FEMs and the V-load analysis methods. Their research focuses on a continuous three-span bridge constructed of five steel I-girders with a noncomposite deck. A field inspection of the bridge determined that the bearings were severely deteriorated and were not allowing the degrees of freedom to be released per design. Relevance of the frozen bearings was explored throughout the FEM.

The study concluded that the detailed FEM produced accurate strain readings under applied live loading. Replacing the frozen bearings with new bearings proved to be negligible because accounting for the amount of resistance provided by frozen bearings is challenging. Another conclusion found that using the V-load for positive moments was 6.8% unconservative for the exterior girders and 8.3% conservative for interior girders when compared to FEM. For negative moments, the V-load was 16.1% conservative for interior

girders and 12% unconservative for exterior girders (Barr et al. 2007). These conclusions might indicate that the V-load method offers a relatively accurate preliminary method of analysis, while FEM analysis would be recommended for final design.

2.3 History of the Design Specifications for Horizontally Curved Bridges

Linzell et al. (2004) discusses the efforts leading up to the formation of the *2003 Guide Specifications for Horizontally Curved Highway Bridges* by AASHTO, hereafter referred to as the *Guide Specs.* The *2003 Guide Specs* encompasses load factor design (LFD) criteria, which will be soon eliminated by the development of the Load and Resistance Factor Design (LRFD) design provisions. Incorporating the LRFD format is anticipated to greatly ease the design of horizontally curved girder bridges.

Through the 1960s curved steel bridges were increasingly designed and constructed as engineers realized their advantages. Because of this, a drive began towards developing the scarcely available specifications and guidelines. This led to the Consortium of University Research Teams (CURT) project managed by the Federal Highway Association (FHWA). The CURT project completed analytical and theoretical work which eventually helped create a preliminary set of specifications for allowable stress design (ASD) which were later accepted by AASHTO in 1976. Through additional work by AASHTO committees and the American Iron and Steel Institute, LFD criteria were developed and transformed from the preliminary set of ASD specifications by CURT. The LFD criteria combined with the ASD criteria formed the 1980 AASHTO *Guide Specs*. After eight revisions, another edition was published in 1993.

The 1993 *Guide Specs* concepts were difficult to understand and could be easily misused by designers. The *2003 Guide Specs* offer more details for discussion of the specifications and include design examples. Design for the *2003 Guide Specs* includes general parameters, preliminary design, preliminary analysis, and refined design as four main categories.

General parameters are broken down into two main divisions of design and construction. The design of the bridge is subdivided into general bridge geometry and limit states that incorporate: strength, fatigue, serviceability, and constructability. Criteria for preliminary design are outlined based on material strengths and girder geometries. Preliminary member sizes and framing can be calculated in accordance to Articles 5, 6, 9, and 12 of the

specifications. As outlined in previous sections, preliminary analysis of a horizontally curved girder bridge can be much more sophisticated than a traditional straight girder bridge. A percentage of the applied load is often transmitted to the girder with the largest radius. Because of this, the entire structure must be analyzed as a whole, in contrast to only analyzing single girders with distribution factors. Often, small-deflection theory can be used for most bridges. Second-order analyses are usually recommended during construction phases and stability checks. If certain requirements are met, the effects of curvature may be neglected when considering vertical bending moments. Torsion and lateral bending must account for curvature effects. The V-load method is recommended for simplified cases outlined in the specifications. Finite element theory is recommended for more refined analysis methods if the criteria for V-load are not met. Finally, design refinement is performed as an iterative process to ensure that all components meet design requirements such as strength, serviceability, fatigue, overload, detailing, and constructability. Allowed processes for design refinement are outlined as mentioned (Linzell et al. 2004).

2.4 Load Distributions for Horizontally Curved Bridges

Kim et al. (2007) studied live load radial moment distribution in horizontally curved girders. As previously stated, substantial normal stresses are present in horizontally curved girders due to warping torsion. Cross frames are designed to reduce these warping normal stresses. These primary members offer an additional load path for induced live loads which has an effect on vertical bending of adjacent girders. Because of this, cross frames and diaphragms will have a significant influence on transferring load from one girder to the next. Transferring of load can be assessed by calculating girder distribution factors (GDF). The Kim et al. report focuses on developing GDF equations which are primarily a function of cross framing details. The research employed both field studies and analytical models. Three increasing levels of complexity for modeling of the FEM were utilized and are shown in Figure 2.3. Based upon field measurements, results showed that Type I was conservative by up to 45%, Type II only differed by 10% and Type III provided slightly more accurate results than Type III. Due to the added increased effort for creating a Type III model, the slightly increased accuracy was deemed negligible. Radius, span length, and cross frames all were found to influence the live load distribution. On the other hand, the parapets and deck

thickness were insignificant with respect to GDFs. Overall, the span length was found to be the most influential factor.
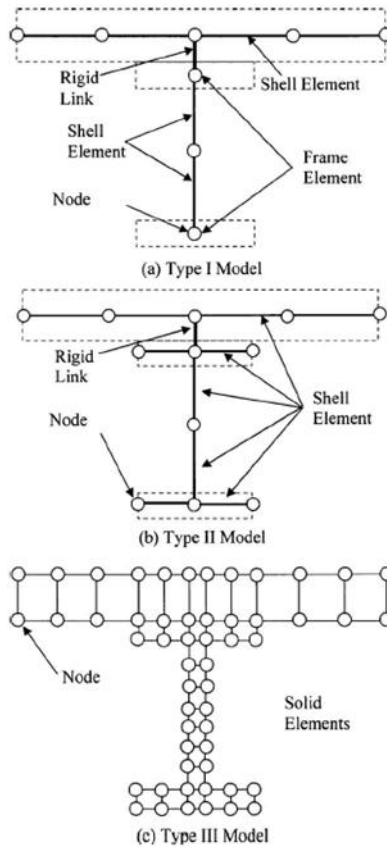
Figure 2.3. Levels of Analysis from Fig. 1 Kim et al. (2007)

A study by Miller et al. (2009), previously mentioned, made conclusions from calculated dynamic amplification factors (DAF). When comparing the FEM analysis to field data analysis, the study found that the FEM overestimated the stiffness of the diaphragm to girder connection as it predicted greater transfer of loads between adjacent girders as compared to field measurements. Consequently, load distribution was greater for the outermost girders. The field results indicated that DAF were within the limit of AASHTO recommendations.

In contrast to the research by Miller et al. (2009), Barr et al. (2007) determined that the FEM distribution factors differed by only 5% from the AASHTO (2003) standard distribution factors. This discrepancy could be due to varying degrees of complexity in each FEM.

2.5 Framing and Erection of Horizontally Curved Girders

Although steel I girders offer minimal torsional resistance, they are most commonly used in the construction of horizontally curved bridges. These members are only stable when connected via diaphragms or cross bracing, which leads to substantial interaction forces in those connecting members. Consequently, the analysis and design of the superstructure needs to accommodate these forces (Linzell et al. 2004).

In a dissertation from the University of Maryland, Thanasattayawibul addresses the two main types of curved girder framing, closed and open framing (Thanasattayawibul 2006). Closed framing resists torsion through the interactions of girders that are connected by diaphragms or floor beams along with lateral bracing at girder flange locations. In contrast, open bracing does not include the horizontal bracing of girder flanges. Combinations of closed and open framing can be used during construction of curved bridges. Examples of such combinations would be exterior girders, where the interior face is connected to adjacent girders and the exterior face is open. Cross frames and diaphragms act as secondary members in straight bridges; however, they act as load-carrying members in curved bridges. The report also notes that spacing of cross frames has a significant effect on warping stresses.

In a presentation, associated with HNTB, LaViolette further highlights the importance of erecting horizontally curved members (LaViolette 2009). He explained that lateral bending is primarily caused by warping normal stresses along with wind loads, skew, and overhangs of girders during construction. Throughout construction and erection phases, many calculations must be made to account for the several stages of construction. Stability of each individual girder and the multi-girder system as a whole must be met. Often, these calculations and checks are made by performing a 3D finite element analysis to investigate each sequence of construction. Structural engineers must account for load capacities and stabilities at all stages of construction. Notable loadings to be accounted for should include self-weights and attachments, wind loads, loads induced during lifting and tie downs, girders rolling due to unbalanced loadings, and several more. Additionally, issues during erection can be prevented by properly noting the alignment. Such preventions include detailing sufficient cross framing, using falsework, properly placing holding cranes, and thoroughly following procedures outlined for pinning, bolting and tightening. A detailed set of erection drawings are extremely important. La Violette states that drawings should include work area plans,

erection sequences, temporary supports, rigging details, etc. Neglecting to follow rigorous construction plans have proven to cause catastrophic failures resulting in injuries and death.

2.6 Integral Abutments and Horizontally Curved Girders

One key factor in general bridge design can be eliminating expansion joints and expansion bearings throughout a bridge structure. The installation and maintenance of bearing joints can be problematic due to leaky joints which result in corrosion and buildup of debris at the bearings. This ultimately results in the performance of the joint failing. Eliminating these joints can potentially decrease maintenance costs and ultimately increase the structure life. In order to eliminate joints and seals, integral abutments were introduced. Integral abutment bridges are designed without joints in the bridge deck. They have stiffness and flexibilities in the soil and supports to resist thermal and braking loads applied to the bridge. These bridges are less expensive to construct, simple to detail in design, and require less maintenance (Mistry 2000).

However, incorporating integral abutments with horizontally-curved girders can be more difficult to understand and analyze as compared to an equivalent straight girder bridge. Doust (2011) assessed the effect of introducing integral abutments to horizontally-curved bridges. The study focused on the live-load response of a curved steel I-girder IAB. Abutment pile moments were found to be approximately 20% larger than an equivalent straight bridge. Direct relationships between abutment pile moments and the bridge's radius or length were not apparent; although, the orientation of the pile with respect to possible bridge skews may be significant and require further investigation beyond the original Doust study.

CHAPTER 3 SHORT TERM INSTRUMENTATION AND DATA COLLECTION PROTOCOL

The contents of this chapter discuss, in detail, the short term live load field testing performed on five of the six bridges at the NEMM. The results of the field testing are presented in Chapter 4. Refer to Shryack et al. (2012) for a detailed description of the long term field instrumentation and data collection protocol.

3.1 Strain Transducer Information

Strain transducers were used to test live load, superstructure behavior of one straight bridge and four horizontally curved bridges at the NEMM. Bridge Diagnostics, Inc. (BDI) strain transducers were used throughout the testing. These temporarily placed transducers are designed to measure load-induced strain on structural members. In this testing, the structural members instrumented were limited to the steel girders of the superstructure of all five bridges. The BDI strain transducers are 3 in. reusable gauges that mount directly to the surface of the structure using adhesive. An example photograph of a mounted transducer is shown in Figure 3.1.

Figure 3.1. Mounted Strain Transducer

The superstructure of each curved bridge was instrumented with 40 strain transducers. Each of the four I-girders was outfitted with four transducers at two separate radial cross-sections. In all cases the first cross-section, Section 1, is located at half the unbraced length between two diaphragms. Section 2 is located where diaphragms are present. Both sections

are parallel to the radius of curvature and adjacent to one another. The instrumented sections of each bridge are illustrated in the plan views of Figure 3.2 through Figure 3.6.
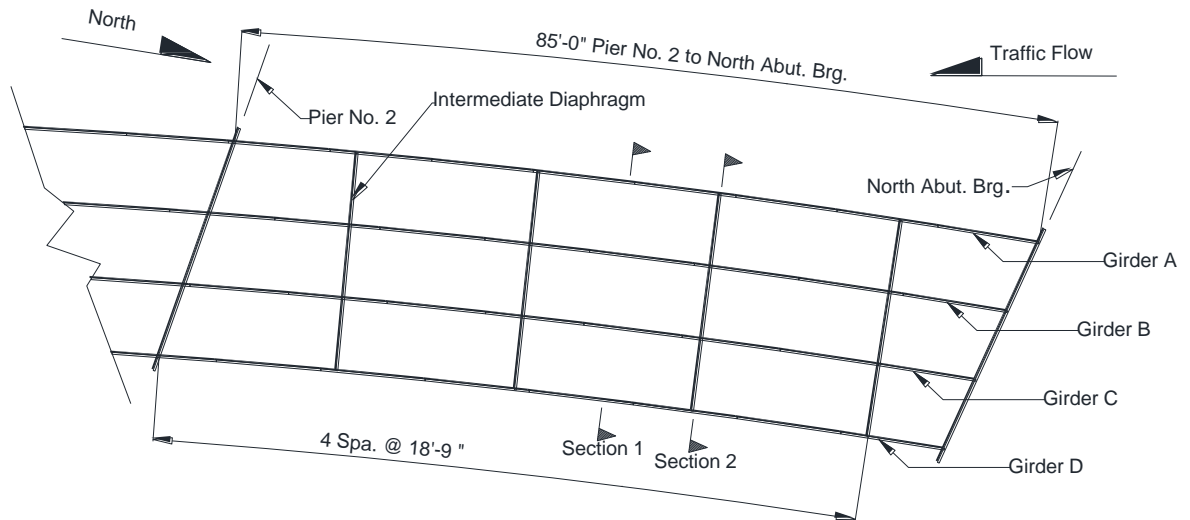
Figure 3.2. Plan View of Bridge 309
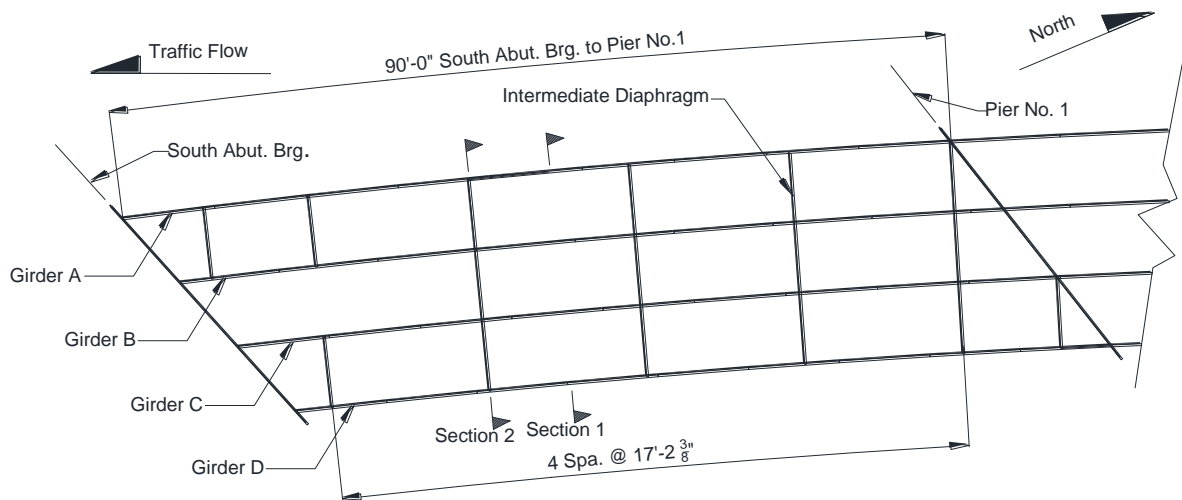
Figure 3.3. Plan View of Bridge 209

16
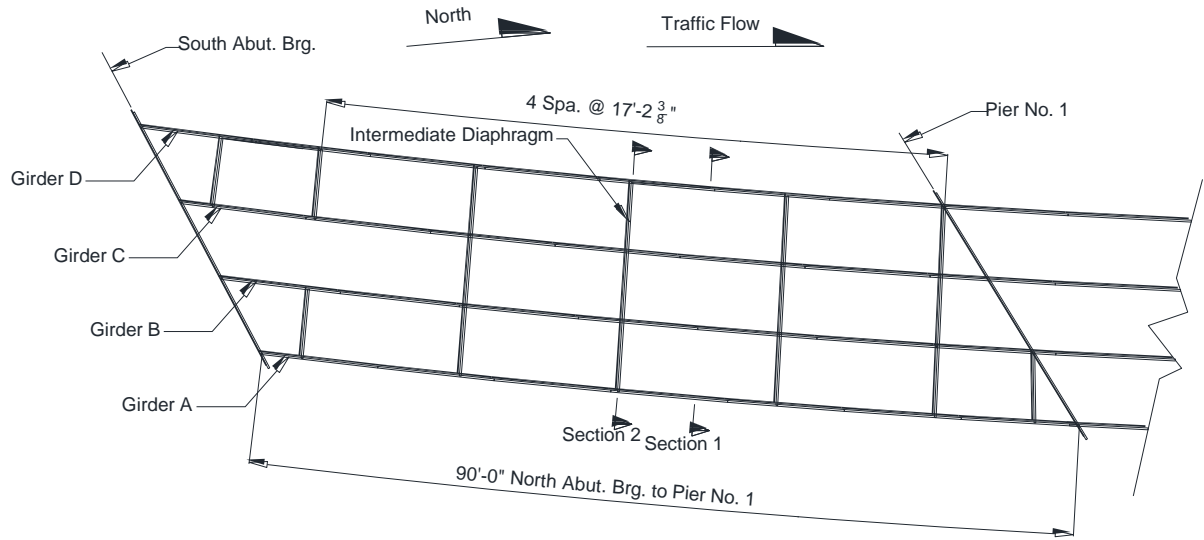
Figure 3.4. Plan View of Bridge 2208
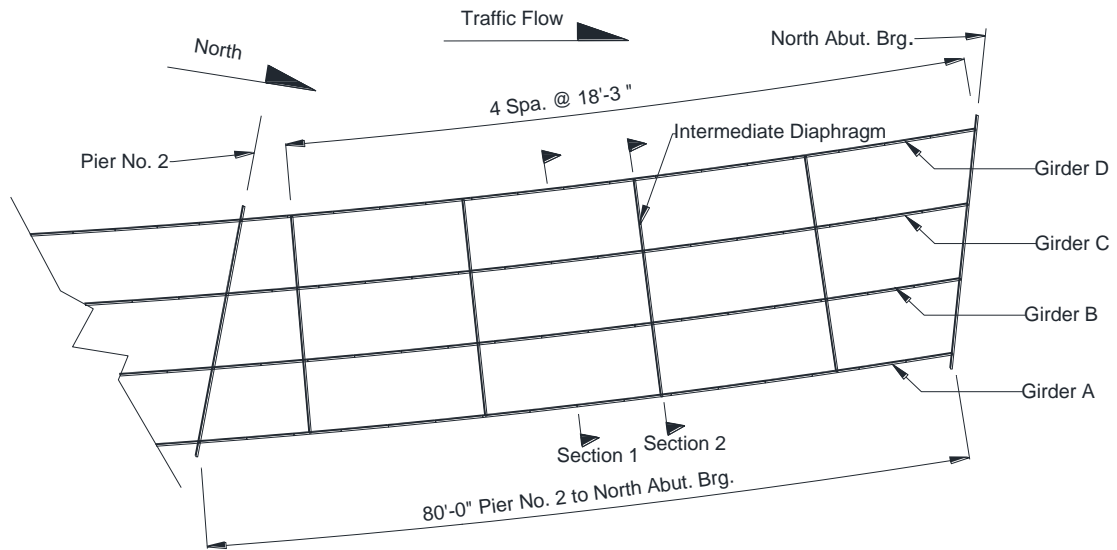
Figure 3.5. Plan View of Bridge 2308

www.manaraa.com
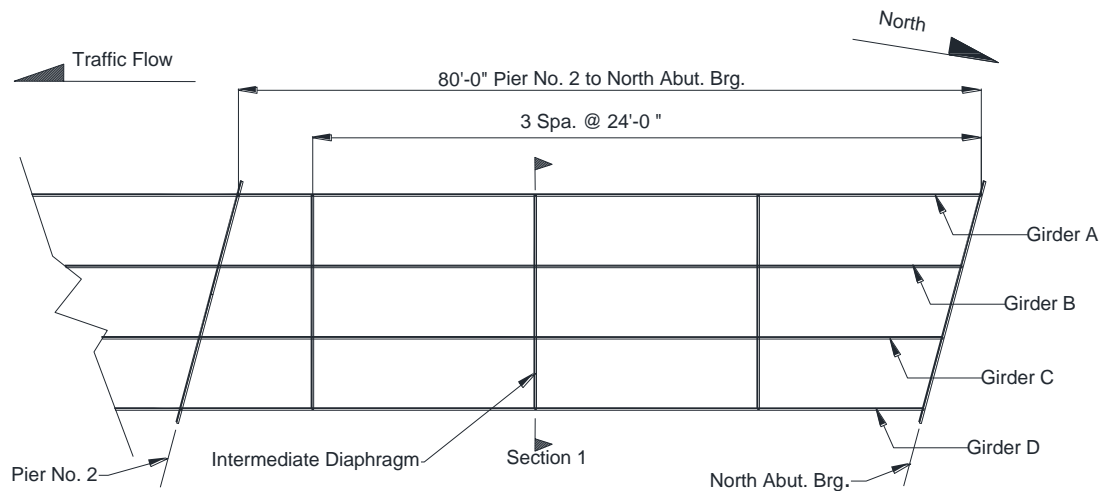
Figure 3.6. Plan View of Bridge 109

Four strain transducers were placed on the upper and lower flanges of each girder at both sections shown in Figure 3.7 and Figure 3.8. In Section 2, the two diaphragms towards the inside of the curve were instrumented with transducers at mid-length. The diaphragm towards the outermost of the curve was instrumented with four transducers located at the one-third points as shown in Figure 3.8. Figure 3.9 displays the detailed placement of the transducers on both the girder and diaphragm flanges.

Only 16 transducers were placed on the only straight bridge tested, Bridge 109. These transducers were installed only at one section. This section is comparable to Section 1 in the curved bridges, where the transducers were placed at half the unbraced length between two cross frame sections as illustrated in Figure 3.6. No Bridge 109 diaphragms or cross frames were instrumented.
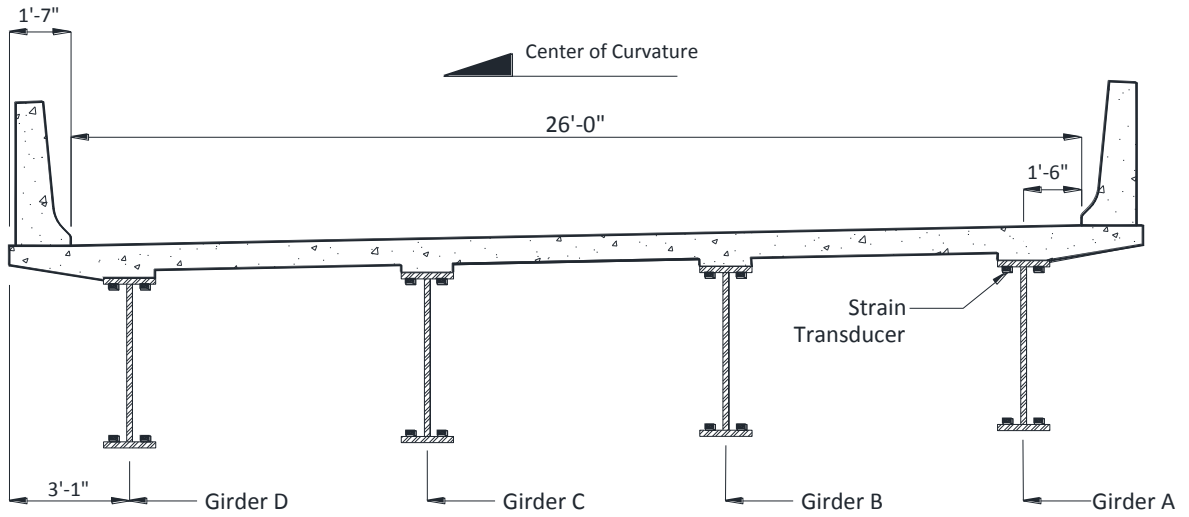
Figure 3.7. Section 1- Strain Transducer Locations
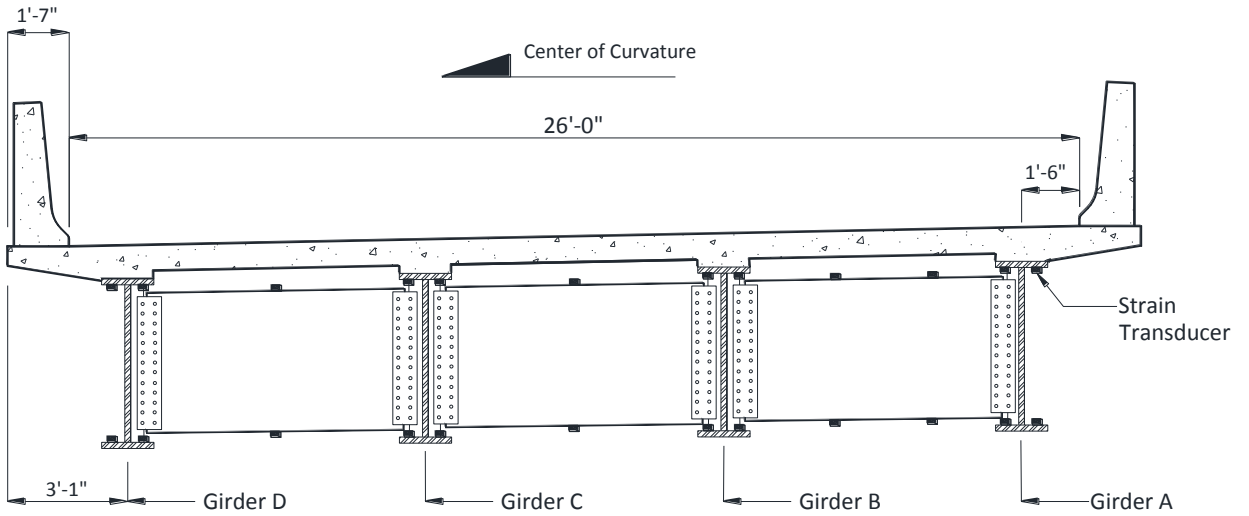
Figure 3.8. Section 2- Strain Transducer Locations
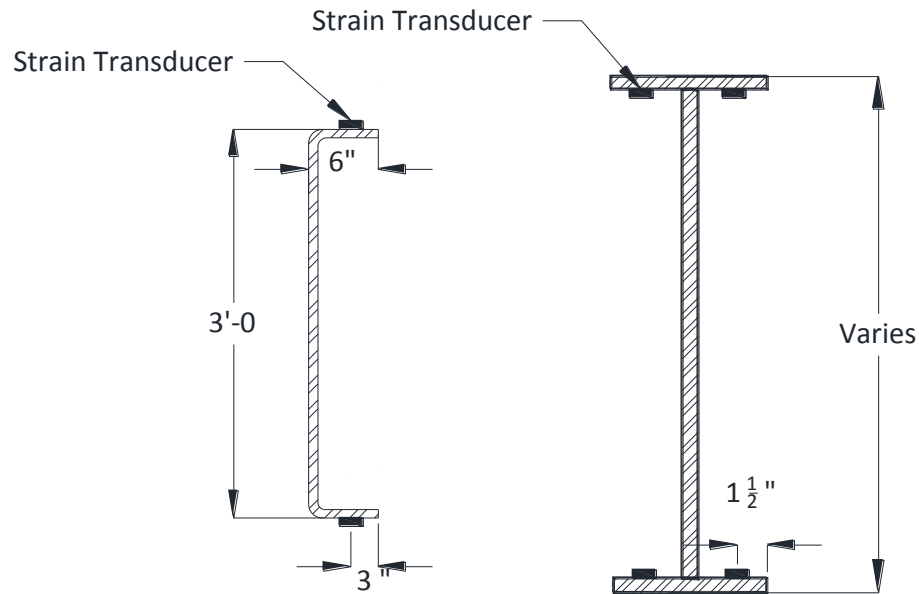
Figure 3.9. I-Girder and Diaphragm Strain Transducer Detail

3.2 Live Load Testing

This section discusses three aspects of live load testing, the test vehicle, load paths, and static and dynamic test procedures.

3.2.1 Test Vehicle

A three-axle Iowa Department of Transportation dump truck was used for live load testing of all five bridges. The test vehicle consisted of three axles, one steer axle and two drive axles. Loaded with gravel, the gross vehicle weight of the truck was approximately 48,700 lb. Individual axle weights along with the gross vehicle weight were recorded at a Certified Automated Truck Scale located in Des Moines, IA. Refer to Figure 3.10 for axle spacing and loading.
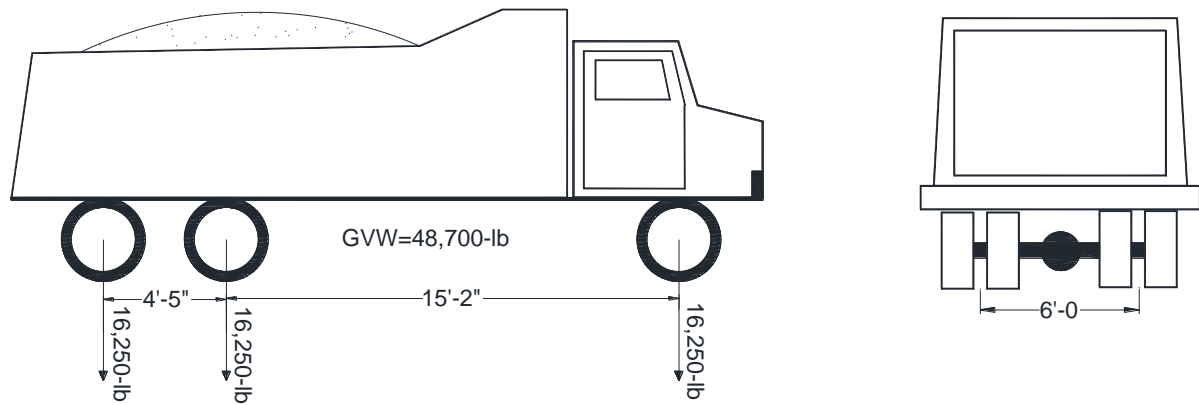
Figure 3.10. Truck Configuration and Loading

3.2.2 Load Paths

Three parallel load paths were pre-defined so as to induce extreme and typical truck positions. The driver-side wheels were placed 2 ft from the inner barrier rail on Load Path 1 (LP1). Load Path 2 (LP2) was centered on the bridge deck. The passenger-side wheels were placed 2 ft from the outer barrier rail on Load Path 3 (LP3). These three paths are outlined in Figure 3.11, which represents a general horizontally curved bridge.

(a)

(b)
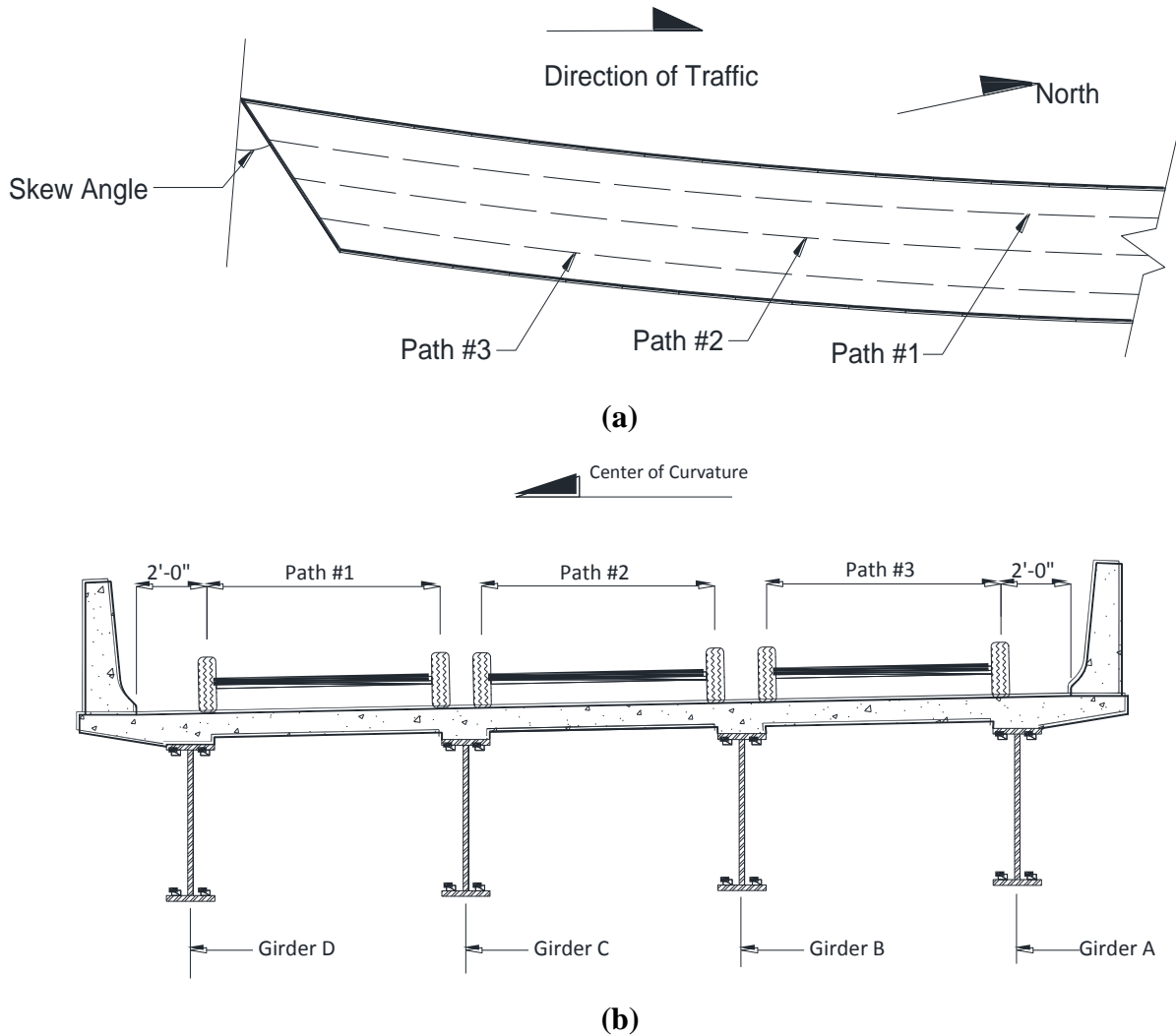
Figure 3.11. (a) Plan View and (b) Cross Section View of Load Path Placement

3.2.3 Static Load Data Collection

Static load testing was conducted for all three load paths. For each trial, the truck travelled across the bridge along the individual load path at a crawl, or walking pace. Each load path consisted of two identical trials to ensure that consistent data were being collected. Hence, six total static load trials were logged.

Prior to collecting data on the acquisition software, each individual strain transducer was zeroed and the sample frequency was set to 20 Hz. Once the testing trials began, longitudinal tracking of the vehicle occurred at 20 ft intervals.

3.2.4 Dynamic Load

Only two trials were conducted for the dynamic load cases. For this testing, the speed of the truck was increased to approximately 35-45 mph. Again, two identical trials were performed to ensure consistent data collection. Load Path 2 was used for both trials. Due to the increased speed, the truck could not be safely placed at a constant 2 ft from the barrier rails; consequently, Load Paths 1 and 3 were not used. Data were collected at 100 Hz. Since the truck was moving at increased speeds, only start and end of bridge truck positions were recorded.

CHAPTER 4 HEALTH MONITORING AND FIELD EVALUATION OF HORIZONTALLY CURVED GIRDER BRIDGES WITH INTEGRAL ABUTMENTS

Modified from a paper prepared for submission to the *Transportation Research Record: Journal of the Transportation Research Board*

Jerad J. Hoffman, Brent M. Phares, and Gus L. Shryack

Abstract

Nationally, questions have been raised about the combined use of integral abutments and horizontally curved steel I-girders. This design is rather new to the Nation. Because of the large number of newly constructed bridges designed with curved steel I-girders and the advantages that integral abutments provide, having a better understanding of this type of bridge is of great importance. The primary objective of this work was to monitor and evaluate the long and short-term behavior of four in-service, horizontally curved, steel I-girder bridges with integral and semi-integral abutments to provide a baseline on general performance. In order to meet the project scope, a monitoring program was developed and deployed on five bridges using an array of strain gauges, pressure transducers, and movement monitors. Results from the collected data, with regards to the live load field testing, indicated that the girder moment distribution factors were heavily influenced by only the degree of curvature in the bridges and the V-Load equation provides a modest preliminary assessment of the lateral bottom flange bending based on the degree of curvature with minimal skew. The long-term assessment indicated that an effective thermal range of 100^0 F may cause up to 12 ksi of additional stress in the girders due to restrained expansion and contraction of the bridge. However, despite the thermal induced stresses in the girders, no noticeable differences were observed between these curved and straight bridges based on varying curvature, skew, or support conditions.

4.1 Introduction

A report published by The National Cooperative Highway Research Program raised

questions regarding the design, fabrication, and erection of horizontally curved steel girder bridges. The major reason for the concerns is that up to one-quarter of the nation's steel girder bridges incorporate curvature in their design. To complicate matters even more, these bridges are being designed with integral abutments. Integral abutments are less expensive to construct, simple to detail in design, and require less maintenance (Mistry 2000). However, incorporating integral abutments with horizontal curvature can be more difficult to understand and analyze as compared to an equivalent straight girder bridge (Doust 2011). Because of the advantages, the combined use of horizontally curved steel girder bridges with integral abutments stands to be a promising design. On the other hand, this combination is relatively new to the Nation. The purpose of the work herein is to investigate the use of integral abutments on curved girder bridges through a monitoring and evaluation program.

The design and analysis of straight, integral-abutment bridges (IABs) has a long and extensive history dating back as far as the 1930's. These bridges came about after the introduction of the Hardy Cross Method, and were considered a viable solution to the downfalls of expansion joints and expansion bearings (Tennessee DOT 1996). Although there has been a tremendous amount of research on the response of straight IABs, less attention has been paid to their horizontally curved counterparts. Research on the use of integral abutments on horizontally-curved bridges is scarce (Hassiotis 2006).

Miller et al. (2009) state that curved beams create twisting effects which result in warping out of plane similar to torsion. This phenomenon is referred to as a bimoment, a product of combined bending and torsional shear. In addition, negligible secondary effects occur when the curved compression flange bows outwards, increasing the degree of curvature. When secondary effects are introduced, lateral bending in the flange results in a variation of bending stresses across the flange width.

Lydzinski et al. (2008) further explain additional complications that arise when analyzing and designing I-girders in curved bridges. Complications range from the individual plates to the constructed girder as a whole. Compared to straight girders, horizontally-curved I-girders are significantly different in the following ways:

- Flange local buckling may differ from the outer to the inner side of the web.
- Local buckling is possible on the inner half of the tension flange.

- S-shaped bending occurs in the web, causing an increase of stress at the web-flange connection.
- Bending and torsion stresses are not decoupled, resulting in lateral bending behavior.

The most recent study to investigate the thermal behavior of horizontally-curved, steel-girder, integral-abutment bridges was done by Doust at the University of Nebraska (Doust 2011). In this study a detailed investigation was conducted into the behavior of horizontally-curved, steel-girder, integral-abutment bridges and horizontally-curved, concrete slab, integral-abutment bridges using finite element analysis. Multiple bridges were modeled with varying horizontal curvatures and total bridge lengths. The study considered the effect of different loading conditions applied to the bridges, namely gravity loads, lateral loads (longitudinal and transverse), temperature effects, concrete shrinkage, and earth pressure. From the investigation, the author concluded that for bridges longer than a specific length, dependent mainly upon bridge curvature, the internal forces due to expansion are smaller in a horizontally-curved bridge than in a straight bridge of similar length. Regarding bridge displacement, the author was able to develop an equation to predict the direction of end displacements of a horizontally-curved, integral-abutment bridge.

Hall et al. (1999) established design specifications for horizontally-curved, steel-girder bridges. This report was part of the NCHRP and was the result of over one hundred studies. Section 3.4 of this report addresses thermal loads in the bridge superstructure. It states:

According to the Recommended Specifications, curved bridges should be designed for the assumed uniform temperature change specified in AASHTO Article 3.16. The orientation of bearing guides and the freedom of bearing movement is extremely important in determining the magnitude and direction of thermal forces that can be generated. For example, sharply skewed supports and sharp curvature can cause very large lateral thermal forces at supports if tangential movements are permitted and radial movements are not permitted. Under a uniform temperature change, orienting the bearing guides toward a fixed point and allowing the bridge to move freely along rays emanating from the fixed point will theoretically result in zero thermal forces. Other load conditions, however, can dictate the bearing orientation. The bearing restrains and orientation, as

well as the lateral stiffness of the substructure, must be considered in a thermal analysis (15).

In addition, in certain conditions there is a need to consider deck temperature gradients as specified by the *2010 AASHTO LRFD Specifications,* referred to as the *AASHTO Specs* hereafter. If the width of the deck is less than one-fifth of the longest span, the bridge is considered narrow and uplift can occur at the bearings. Section 8.3 of the Hall et al. report addresses thermal induced movements in the bearings and states "Bearing devices should be designed to accommodate movements due to temperature changes in the superstructure and to accommodate rotations about the tangential and radial axes of the girder" (25).

Moorty and Roeder (1992) studied the effect various geometric parameters, orientation of the bearings, and the stiffness and resistance of the substructure had on the thermal response of curved bridges. Analytical models of a 600-ft long, three span, horizontally-curved, steel-girder bridge had vertically varying temperature distributions applied to them. Moorty and Roeder were able to draw a number of conclusions about the design of horizontally-curved, steel-girder bridges, as noted here. The method of predicting thermal movements recommended by the *AASHTO Specs* is reasonably for straight orthogonal bridges, but a more refined analysis may be required for skew and curved bridges. An increase in the curvature of the bridge results in an increase in the radial movements and the stresses in the bridge. The relative stiffness of the bridge, the girder bearings, and the substructure influence the tangential and radial movements in a horizontally-curved bridge; and the transverse movements and stresses in bridges increase with an increase in the skew angle and the width of the bridge.

4.2 Experimental Procedure

The re-alignment of the intersection of Interstates I-35, I-80 and, I-235 (Northeast Mix-Master) included the construction of six new bridges, including four curved girder bridges with integral or semi-integral abutments. With the construction of these new bridges, a unique opportunity was presented to investigate the previously stated issues.

Working with the Iowa DOT Office of Bridges and Structures, the research team developed preliminary instrumentation schemes for five of the six new Northeast Mix-Master (NEMM) bridges. The instrumentation layouts relevant to topics discussed in this paper

typically consisted of strain transducers on the steel girders along with various temperature, pressure, and displacement sensors.

The bridges were monitored over a period of approximately 15 months for assessing the long-term thermal behavior. During this period, the strains, temperatures, and displacements were recorded once per hour under varying thermal conditions. In addition to the long-term monitoring, a short-term assessment was conducted by performing a series of live load tests and measuring superstructure responses using an array of strain transducers placed on the steel girder flanges.

Using the collected data, simple analytical models and observations were formulated. The goal was to relate the results to several design conditions (e.g., geometry, boundary conditions, etc.) that may provide information on other hypothetical situations.

4.2.1 Site Description

There were five, three-span bridges at the NEMM that were included in this study. The interchange layout was configured such that semi-integral abutments were used in two of the curved bridges and integral abutments were used in the other two curved bridges. The final bridge is straight with integral abutments and was generally used for comparison purposes. Table 4.1 lists the length, width, skew angle, curve, radius, spans, abutment type, and pier fixity for each bridge.

Table 4.1. NEMM bridge geometry

Design No.	109	209	309	2208	2308
Length (ft)	304	332	319	330	302
Width (ft)	26	26	26	26	26
Skew (°)	15	35	15	35	15
Radius (ft)	N/A	1340	950	1340	950
Spans (ft)	80-144-80	90-152-90	85-149-85	90-150-90	80-142-80
Abut. Type	Integral	Semi-Integral	Integral	Integral	Semi-Integral
S. Pier Fixity	Expansion	Fixed	Fixed	Expansion	Fixed
N. Pier Fixity	Fixed	Expansion	Fixed	Fixed	Fixed

4.2.2 Bridge Cross Section

Except for the girder dimensions and diaphragm configuration, the cross-sectional properties for all six bridges are similar. All five bridges were constructed with welded, I-

shaped, plate girders. The horizontally curved bridges have non-composite bent plate diaphragms and the straight bridge has cross frames with WT horizontal members and angle diagonal members. A typical bridge cross section is shown in Figure 4.1(a). The left half of the figure shows the diaphragm configuration for the horizontally curved bridges and the right side of the figure shows the cross frames of the straight bridge.
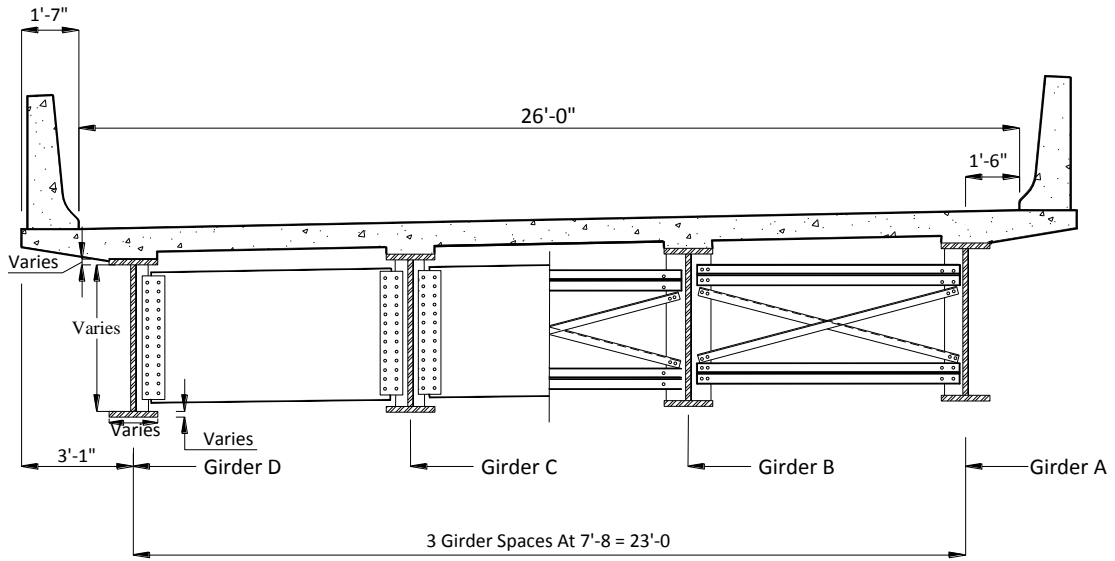
(a)
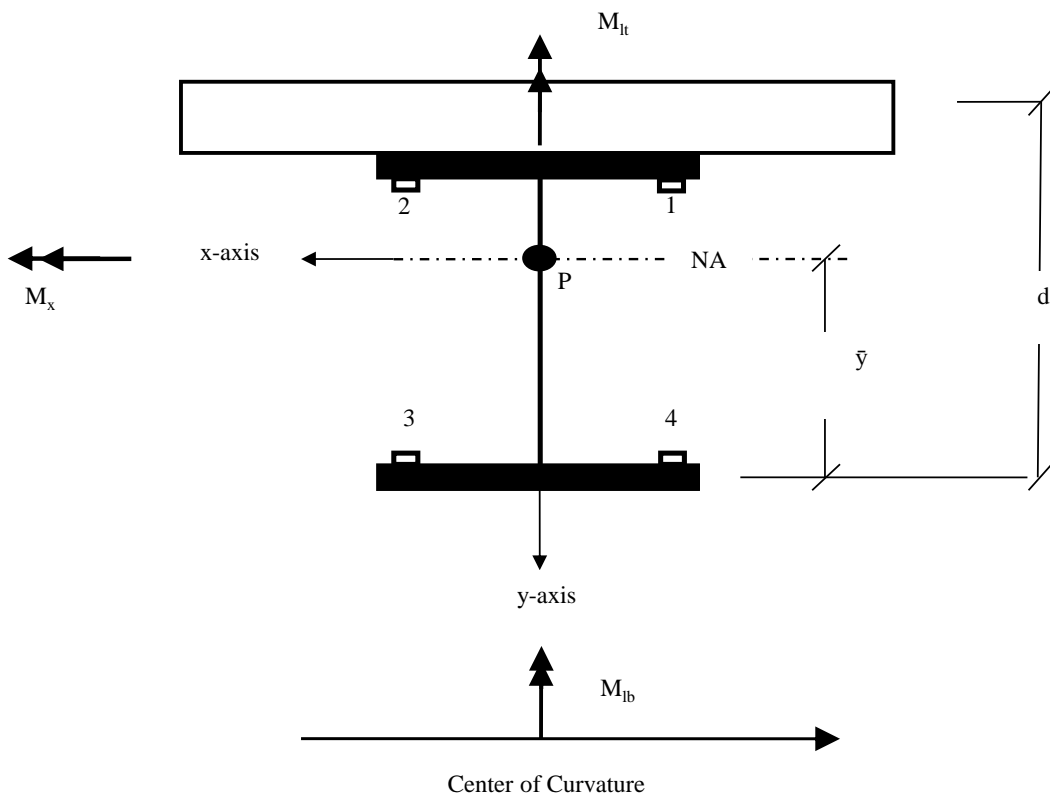
(b)

Figure 4.1. (a) Typical cross section (b) Composite girder section with member forces

In this work, the exterior girder on the outside of the curve has been labeled Girder A and the exterior girder on the inside of the curve has been labeled Girder D. The straight bridge is labeled in a similarly consistent manner. Girders B, C, and D in the curved bridges have the same steel cross sectional properties, while Girder A has a larger moment of inertia about the strong axis by up to 20%.

4.2.3 Short-term Assessment

For the short-term assessment, the superstructure of each curved bridge was instrumented with 40 strain transducers at approximately mid-span of an end span. Each of the four I-girders was outfitted with four transducers at two separate radial cross-sections. Four strain transducers were placed on the upper and lower flanges of each girder at both sections. In all cases the first cross-section, Section 1 (S1), is located at half the distance between two diaphragms. Section 2 (S2) is located at a diaphragm. Both sections are parallel to the radius of curvature and adjacent to one another.

Only 16 transducers were placed on the straight bridge, Bridge 109. These transducers were installed only at one section. This section is comparable to Section 1 in the curved bridges.

A three-axle dump truck was used for live load testing of all five bridges. The gross vehicle weight of the truck was approximately 48,700 lb. Three parallel load paths were pre-defined so as to induce extreme and typical truck loading conditions. The driver-side wheels were placed 2 ft from the inner barrier rail on Load Path 1 (LP1). Load Path 2 (LP2) was centered on the bridge deck. The passenger-side wheels were placed 2 ft from the outer barrier rail on Load Path 3 (LP3).

4.2.4 Long-term Assessment

For this work, vibrating-wire strain-gauges measured strains at mid-length of select girders and spans. Only the exterior girders (Girder A and Girder D) were monitored for each bridge. All four horizontally curved bridges were monitored at each span and the straight bridge was monitored at mid-span of the center span only. Again, each monitored girder was outfitted with four gauges on the upper and lower flanges.

In addition to the strain, ambient air and steel temperature was recorded using a vibrating-wire sensor. Also, temperature gauges were placed at mid-depth of the bridge decks

to measure the internal concrete temperatures.

4.2.5 Member Strains and Forces

The data collected from the strain gauges were used to calculate the internal strains and forces induced in each monitored member due to the truck loading and ambient temperature changes. Utilizing the specific girder cross sectional properties and elementary beam theory, the four measured strains at each girder cross section were resolved into the four force-related strains and the four girder forces as calculated by Section 6.2 in Shryack et al. (2012). Figure 4.1(b) depicts the forces considered in analysis of the composite section. The forces were chosen to align with the *AASHTO Specs* codified approach for calculating lateral forces due to live loading (AASHTO 4-3).

Referencing Figure 4.1(b), the internal forces induced on a girder cross section are as follows:

- P = axial force, tension is positive
- M_x = strong axis bending, positive when the top flange is in compression
- M_{lt} and M_{lb} = lateral bending of the top and bottom flange, respectively; as is prescribed in the *AASHTO Specs*, tension in the flange tip on the outside of the curve is considered positive.

<p align="center">**4.3 Short-term Field Results**</p>

The live load behavior was assessed using point-in-time testing and therefore much of the collected data were plotted versus truck position. Observations and conclusions throughout this section were based on values summarized in tables that were generated from analyses presented in the as of yet unpublished report from the Iowa State University Institute for Transportation (Intrans) by Phares et. al (2013).

4.3.1 Girder Forces

Initially, plots were created that graphed the four measured strains on the girder flanges versus truck position. These plots were produced for each of the five bridges due to each of the three load paths, LP1, LP2, and LP3. The data produced several observations that were pertinent to the four curved bridges. These observations were then further addressed by computing the member forces previously outlined. Further investigation utilized the

components of lateral flange bending, strong axis bending, and axial loads in the girders. For the scope of this paper, only strong axis bending moments and lateral bottom flange bending moments are discussed.

Strong axis bending moment

Table 4.2 tabulates the maximum strong axis bending moments and the associated load path in each girder for the five bridges.

Table 4.2. Maximum M_x and M_{lb} (kip-in.)

	Girder	**Bridge Section 1 (S1)**				**Bridge Section 2 (S2)**			
		A	**B**	**C**	**D**	**A**	**B**	**C**	**D**
M_x (kip-in.)	309	1840[LP3]	1620[LP3]	1400[LP1]	1580[LP1]	1510[LP3]	1680[LP2]	1670[LP2]	1530[LP1]
	2308	1870[LP3]	1530[LP3]	1350[LP2]	1570[LP1]	1510[LP3]	1350[LP2]	1240[LP2]	1130[LP1]
	2208	1340[LP3]	1340[LP3]	1210[LP2]	1210[LP1]	1300[LP3]	1320[LP2]	1340[LP2]	1180[LP1]
	209	1580[LP3]	1600[LP3]	1370[LP2]	1480[LP1]	1090[LP3]	1450[LP3]	1280[LP2]	820[LP1]
	109	1310[LP3]	1560[LP3]	1600[LP2]	1530[LP1]	-	-	-	-
M_{lb} (kip-in.)	309	-15[LP3]	-7[LP3]	-7[LP2]	-19[LP1]	11[LP2]	8[LP2]	8[LP1]	17[LP1]
	2308	-8[LP3]	3[LP1]	34[LP1]	-17[LP1]	8[LP2]	6[LP2]	10[LP1]	10[LP1]
	2208	-8[LP3]	-4[LP3]	-5[LP1]	18[LP1]	14[LP3]	15[LP2]	6[LP1]	-16[LP1]
	209	-6[LP3]	-6[LP3]	-8[LP3]	-5[LP2]	9[LP2]	-8[LP1]	-13[LP1]	-7[LP1]
	109	-3[LP1]	-12[LP3]	-5[LP1]	4[LP1]	-	-	-	-

These results indicate noticeable strong axis bending moment differences between girders for various bridge geometries. The most significant factors influencing the differences may relate to bridge radius and diaphragm location. Live load distribution factors may be the direct reason for the changes in strong axis moments from one girder to the next. The effects of the various bridge geometries will further be addressed under the live load distribution section.

LP1 (inner path) typically produced the largest M_x in Girder D (inner girder). LP2 (center path) typically produced the largest M_x in Girders B and C. And LP3 (outer path) typically produced the largest M_x in Girder A (outer girder). The largest strong axis moments occurred at S1 in Girder A for the two bridges with the most severe curvature, Bridges 309 and 2308. Also at S1, Girder C had the least moment of all four girders for all curved bridges. For

Bridges 209 and 2208, with less curvature, more uniform moments were produced throughout the four girders at S1. Additionally, the moment in Girder A was less at S2 compared to S1 for all curved bridges. The straight bridge, Bridge 109, produced the largest moments in the interior two girders and the smallest moments in the exterior two girders.

Lateral flange bending moment

As expected and illustrated by Table 3.1, lateral bottom flange bending proved to be more significant in the four curved bridges compared to the straight bridge. Maximum bottom flange moments were as much as three times larger in the curved girders than the straight girders. The largest differences were in Bridges 309 and 2308, which have the largest curvature. These results indicate that increased skew and curvature have direct influences on lateral bottom flange bending. Lastly, the direction of lateral bottom flange bending is apparently related to the diaphragm location, which is further discussed.

4.3.2 Live Load Distribution

Live load distribution was assessed by calculating moment distribution factors for strong axis bending in the four girders for single lane and multi-lane loadings for from the LP1, LP2, and LP3 results.

The live load moment distribution factor due to individual load paths was calculated using equation 4.1.

$$MDF_i = M_{xi}/\Sigma M_x \qquad (4.1)$$

where,

M_{xi} = strong axis bending moment in girder *i*

MDF_i = moment distribution factor in girder *i*

ΣM_x = sum of strong axis moments in all girders at section

The results of equation 4.1 were then plotted versus truck position. This process was repeated for every load path at both S1 and S2. To avoid the localized effect the concentrated wheel loads have on the top flange data, values at either section were selected when the front axle was at least one truck length past the instrumented section.

Since the roadway width was 26 ft for all bridges, 12 ft design lane widths allows two trucks to be placed adjacent to one another. Consequently, multi-lane live load moment distribution factors were approximated by superimposing the results from LP1 and LP3 as these two truck positions could coexist adjacent to each other. Similarly to the single lane moment distributions, the values for the multi-lane loading were selected at one truck length past the instrumented section. Figure 4.2 graphically represents of the controlling values determined for multi-lane MDF's for each girder in all five bridges.
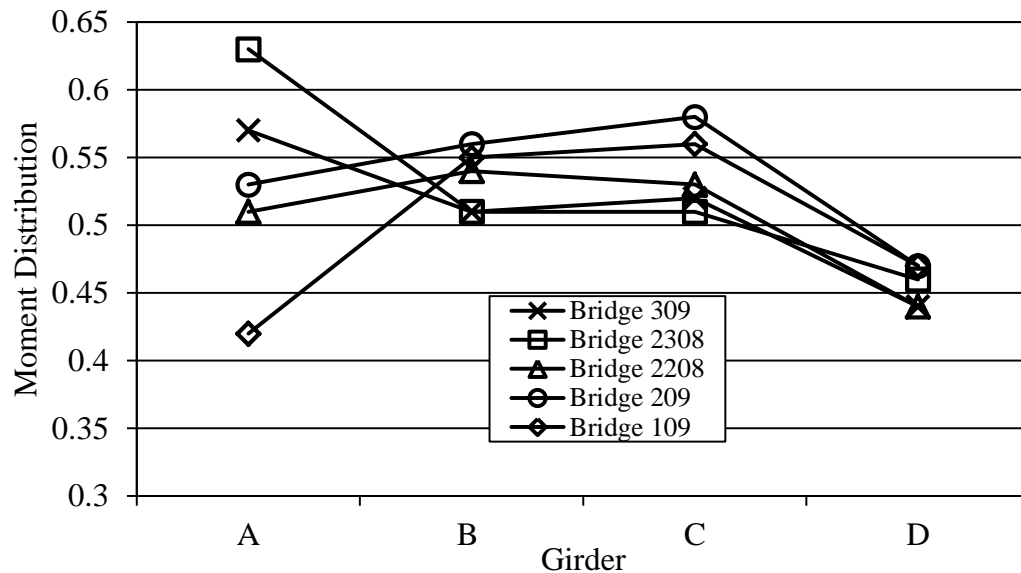
Figure 4.2. Maximum moment distribution factors in bridges

Results in Figure 4.2 indicate the largest MDF's were in exterior Girder A for the two bridges with the most severe curvature, Bridges 309 and 2308, with values of 0.57 and 0.63, respectively. The interior girders produced MDF values ranging from 0.51 to 0.52. Lastly, Girder D produced the smallest moment distribution factors of 0.44 and 0.46 in Bridges 309 and 2308, respectively. Results show the bridges with the largest degree of curvature will distribute more load to the exterior girder located on the outside of the curve and the least amount to the exterior girder located on the inside of the curve.

For Bridges 2208 and 209, which consist of larger radii and skew angles, results were more similar to Bridge 109 than the other two curved bridges. The largest MDF was found in the interior two girders for Bridges 2208, 209, and 109. Values for Girders B and C ranged from 0.53 to 0.58. The exterior girders in Bridges 2208 and 209 produced smaller MDF's,

ranging from 0.44 in Girder D to 0.53 in Girder A. However, Girder A was found to produce larger MDF's than Girder D for these two bridges.

As a general comparison, the experimental MDF's were compared to the approximate method of analysis as specified by Section 4.6.2.2.2 in AASTHO, even though these bridges do not meet the criteria for applying the approximate level of analysis because not all girders have the same stiffness and the degree of curvature exceeds the limits as required in Section 4.6.1.2.4. By applying appropriate bridge geometry, the multi-lane MDF from AASTHO for Bridge 309 equals 0.582 for both exterior girders and 0.623 for both interior girders. Experimental MDF's in the innermost exterior girder, Girder D, for the bridges with the smallest radii are approximately 30% smaller than outermost exterior girder, Girder A.

4.3.3 V-Load Method Example

The well-known V-Load method was explored for lateral flange bending in these curved bridges. The *AASHTO Specs* refer to equation 2.1, the V-Load equation, to determine the lateral flange bending due to curvature for all curvatures. This method is sometimes used in place of a refined method of analysis. Note that the V-Load equation does not account for skew, this may be important as it has been observed here that increasing skew may increase lateral flange bending.

For convenience, the V load equation was rearranged as equation 4.8 to produce the ratio of lateral flange bending to strong axis bending to ease comparison with experimental results.

$$M_{lb}/Mx = L^2/NRD \tag{4.8}$$

Table 4.3 provides the results in equation 4.8 by using an N value of 10 and given bridge geometries. The skew angle of the bridge is listed to provide further information for analysis of the results.

Table 4.3. Results from *AASHTO Specs* equation C4.6.1.2.4b-1 and average field results

Bridge #	Radius, R (ft)	Web Depth, D (ft)	Skew (degrees)	Diaphragm Spacing, L (ft)	M_{lb}/M_x from AASHTO (%)	M_{lb}/M_x from Field (%)
309	950	4.0	15	18.75	*0.9*	*1.0*
2308	950	4.0	15	18.70	*0.9*	*0.8*
2208	1340	3.5	35	17.50	*0.7*	*1.0*
209	1340	3.5	35	17.20	*0.6*	*1.1*

Field results were used to plot the lateral bottom flange bending moment to strong axis bending moment ratios. Since the V-Load equation is only applicable near a diaphragm, only ratios at S2 were considered. Maximum values were then selected from LP1, LP2, or LP3. The average values of the four girders are in the last column of Table 4.3.

Overall, results indicate that the V-Load equation provides a worthy preliminary assessment for the lateral bottom flange bending moment based on the strong axis moment produced in the girder. Average field results at S2 compared well with the V-Load equation results for Bridges 309 and 2308. These two bridges have smaller skews of only 15^0. On the other hand, average values in Bridges 2208 and 209 were greater than the *AASHTO Specs* results in Table 4.3. This increase could be a direct result of the 35^0 skew in these bridges. Additional analysis would need to be performed in order to address the effects of increased skew angles. The V-Load method may help a designer understand the basic behavior of the diaphragm and lower girder flange, even if the numerical results may not be accurate enough for final design. This fact likely becomes more imperfect for smaller radii and larger skews.

4.4 Long-term Field Results

As mentioned, the long-term field monitoring study collected data over the course of 15 months. Strains and temperatures were measured in both the steel girders and concrete deck of the bridge in order to assess the superstructure behavior. In doing so, an effective bridge temperature was established to further interpret the collected strain data. Inferences were drawn from internal girder stress components, which were calculated from the strain components defined previously.

A reference date was selected at 6 a.m. April 28th, 2011 to zero the data. For further information on this topic, refer to the unpublished report on *Field and health monitoring of curved girder bridges with integral abutments* (Phares et. al 2013).

4.4.1 Superstructure

Figure 4.3(a) though Figure 4.3(d) show the internal axial, strong axis bending, top flange lateral bending, and lower flange lateral bending, strains, respectively, versus the effective bridge temperature at the center span of Girder D of Bridge 309. Note that these strains represent the strain resulting from the restraint of thermal changes. In each figure, the light grey data shows the strain for the entire recording period and the black data with white highlights shows the strain for single days with squares representing a low temperature day, circles representing a moderate temperature day, and triangles representing a high temperature day.
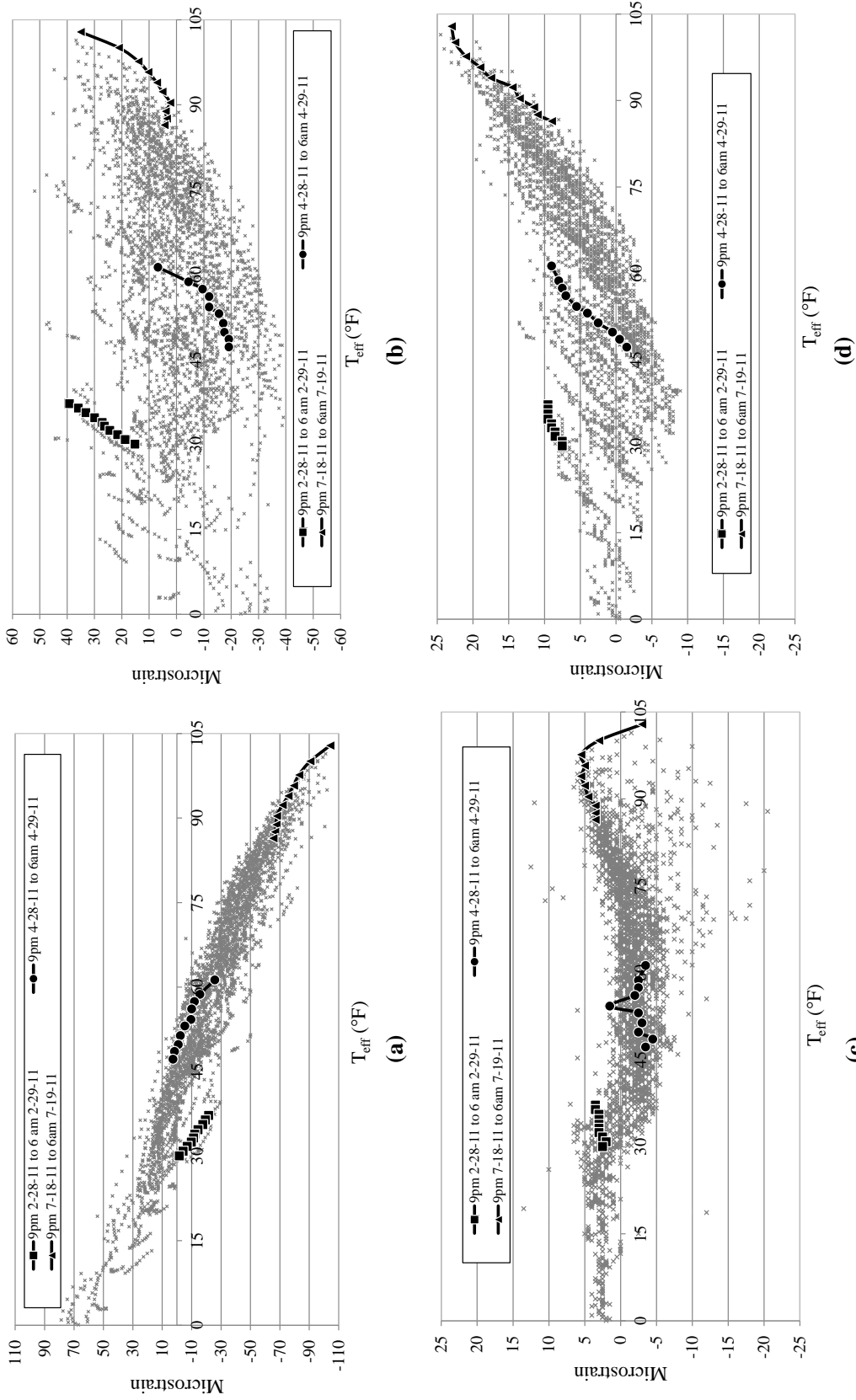
Figure 4.3. Strain components of (a) Axial strain, (b) Strong axis bending strain, (c) Top flange lateral bending, and (d) Bottom flange later bending vs. T_{eff}

Axial strain exhibits a generally linear relationship with the daily and annual effective bridge temperature cycles, and the daily range for axial strain is small compared to the annual range for axial strain. The relationship between strong axis bending strain and the annual effective temperature cycle is difficult to describe. However, the daily range for strong axis bending strain is comparable to the annual range and displays a consistent, non-linear, relationship. This trend is probably due to the thermal gradient induced during the day. Top and bottom flange lateral bending strain display a smaller daily and annual strain range compared to axial and strong axis bending strains. Top flange lateral bending strain is consistently between 5 and -5 microstrain but with no obvious relationship with temperature. Bottom flange lateral bending strain shows a somewhat linear relationship with daily effective temperature cycles, the range of which is in proportion to annual effective temperature cycles.

The range of strain in each girder location was determined based on an equivalent effective temperature, T_{eff}, range of approximately 100 °F. This was the range of effective temperature that the bridge experienced over the course of one year. Once the strain range was established, the resulting corresponding stress ranges were calculated using the modulus of elasticity for steel. Results are tabulated in Table 4.4. Values not available are referenced by "NA".

Table 4.4. Stress ranges

		Bridge #	S span	C span	N span	Avg.
Girder D stress components (ksi)	σ_a	109	NA	5.2	NA	*5.2*
		209	5.2	5.8	5.2	*5.4*
		309	3.8	5.2	5.2	*4.7*
		2208	4.1	3.5	2.3	*3.3*
		2308	5.5	6.4	4.1	*5.3*
	σ_x	109	NA	2.0	NA	*2.0*
		209	3.2	0.6	2.6	*2.1*
		309	2.3	2.0	2.3	*2.2*
		2208	2.6	2.0	2.3	*2.3*
		2308	1.7	2.9	1.0	*1.9*
	σ_{lt}	109	NA	1.2	NA	*1.2*
		209	0.3	1.5	0.6	*0.8*
		309	0.9	0.3	1.2	*0.8*
		2208	0.4	0.3	1.2	*0.4*
		2308	0.4	0.6	2.0	*1.0*
	σ_{lb}	109	NA	0.3	NA	*0.3*
		209	0.9	1.0	0.3	*0.7*
		309	0.4	0.9	0.7	*0.7*
		2208	3.5	NA	0.4	*2.0*
		2308	NA	2.6	1.7	*2.2*
Girder A stress components (ksi)	σ_a	109	NA	5.2	NA	*5.2*
		209	4.4	4.5	4.4	*4.4*
		309	4.9	4.6	4.9	*4.8*
		2208	2.0	2.5	3.5	*2.7*
		2308	3.8	4.4	2.3	*3.5*
	σ_x	109	NA	2.0	NA	*2.0*
		209	2.3	2.3	2.3	*2.3*
		309	1.5	1.2	1.5	*1.4*
		2208	3.2	2.3	2.9	*2.8*
		2308	1.7	1.7	2.9	*2.1*
	σ_{lt}	109	NA	1.7	NA	*1.7*
		209	2.9	0.7	0.7	*1.5*
		309	0.6	0.4	0.4	*0.5*
		2208	0.3	1.2	NA	*0.7*
		2308	1.2	0.3	1.7	*1.1*
	σ_{lb}	109	NA	NA	NA	*NA*
		209	NA	0.6	NA	*0.6*
		309	NA	NA	0.4	*0.4*
		2208	0.6	NA	0.6	*0.6*
		2308	0.9	0.3	NA	*0.6*

The measured internal axial stresses, σ_a, for each of the five bridges are roughly the same (4.4—5.0 ksi). The stress values are somewhat larger for semi-integral abutments and the center span strain is somewhat greater when between two fixed piers.

The strong axis bending stresses, σ_x, for each of the five bridges are in the range of 1.7 to

2.6 ksi. The measured results at the center span of the horizontally curved bridges are typically very close to the measured results at the center span of the straight bridge. The inside girder results of Bridge 109 are lower than the inside girder results of Bridge 309 and Bridge 2308 and are similar to the results of the inside girder results of Bridge 209 and Bridge 2208. The outside girder results are lower than the outside girder results of Bridge 209 and Bridge 2208, and are similar to the outside girder results of Bridge 309 and Bridge 2308.

The measured internal top flange lateral bending stresses, σ_{lt}, at the center of each span for each of the five bridges are all roughly equivalent (0.6 to 0.9 ksi), with some outliers. There are no notable differences with respect to bridge radius or skew, and the results from the straight bridge are only slightly higher than the results from the horizontally curved bridges.

The measured internal bottom flange lateral bending stresses, σ_{lb}, at the center of each span for each of the five bridges are similar to the results of top flange lateral bending stresses; typically around 0.6 to 0.9 ksi. As with top flange lateral bending, there are no notable differences between the straight and curved bridges and no notable difference with respect to bridge radius or skew.

4.4.2 Combined Effects of Thermal and Live Loading

To fully appreciate the magnitudes and effects of the stresses developed by either the live loads or thermal loads, the stresses for each load were tabulated in Table 4.5 for the four curved bridges. Only the exterior girders, Girder A and Girder D, were compared at one of the instrumented end spans of the respective bridge. The maximum live load stress results were magnified by superimposing the outside load path results with the inside load path results. In addition, the stress results from the 48.7 kip test truck were proportionally increased by 48% to obtain approximate results of the 72 kip HS20 design truck. Note that this proportional increase only accounts for the increase in gross vehicle weight. Lane loads, multiple presence factors, or impact factors were not considered in this comparison. The combined loading stress was calculated and listed in the right column of the table. The total stress, σ_{total}, in the bottom flange was also calculated and listed in the table.

Table 4.5. Maximum live load and thermal load stresses in exterior girders

		Bridge #	LL	Thermal	Combined Loads
Girder A stress components (ksi)	σ_a	209	0.6	4.4	*5.0*
		309	0.5	4.9	*5.4*
		2208	0.6	2.0	*2.6*
		2308	0.6	2.3	*2.9*
	σ_x	209	2.3	2.3	*4.6*
		309	2.3	1.5	*3.8*
		2208	1.9	3.2	*5.1*
		2308	2.5	2.9	*5.4*
	σ_{lb}	209	0.1	NA	*0.1*
		309	0.2	0.4	*0.6*
		2208	0.1	0.6	*0.7*
		2308	0.2	NA	*0.2*
	σ_{total}	209	3.0	6.7	*9.7*
		309	3.0	6.8	*9.8*
		2208	2.6	5.8	*8.4*
		2308	3.3	5.2	*8.5*
Girder D stress components (ksi)	σ_a	209	0.7	5.2	*5.9*
		309	0.6	5.2	*5.8*
		2208	0.6	4.1	*4.7*
		2308	0.7	4.1	*4.8*
	σ_x	209	2.2	3.2	*5.4*
		309	2.1	2.3	*4.4*
		2208	1.7	2.6	*4.3*
		2308	2.4	1.0	*3.4*
	σ_{lb}	209	0.1	0.9	*1.0*
		309	0.2	0.7	*0.9*
		2208	0.4	3.5	*3.9*
		2308	0.4	1.7	*2.1*
	σ_{total}	209	3.0	9.3	*12.3*
		309	2.9	8.2	*11.1*
		2208	2.8	10.2	*13.0*
		2308	3.5	6.8	*10.3*

Note that the stresses presented in Table 4.5 represent only a portion of all loading conditions to be considered in design. However, with that said, these experimental results can

aid in better understanding the significance of the behavior of a horizontally curved girder bridge with integral abutments under live loading and thermal loading conditions. Results in Table 4.5 show that thermal loads yielded the largest total stresses of the two loading conditions. The maximum thermal case of 10 ksi occurred in Girder D (the innermost girder) for Bridge 2208. On average, the thermal stresses accounted for approximately 70% of the total combined loading stresses in each of the exterior girders. Thus, these experimental results indicate that thermal loading would be a critical condition to account for when designing the superstructure of bridges with integral and semi-integral abutments. Again, with the results presented in Table 4.5, no notable differences were found when relating the thermal stress magnitudes to the degree of curvature or skew of these particular bridges.

4.5 Discussion and Conclusions

Based on the results from the field testing and associated assessment, the research team developed several conclusions about the behavior of curved girder, integral abutment bridges with respect to both live loads and thermal loads. Regarding the live load behaviors:

- The live load moment distribution factors of curved integral abutment bridges are most notably influenced by the degree of curvature.
- The largest MDFs were found in exterior Girder A (girder on outside of curve) for the two bridges with the most severe curvature.
- The V-Load equation may notably underpredict the magnitude of M_{lb} as skew angles increase.
- The superstructure behavior of these bridges under live load conditions can only be preliminarily analyzed from the simplified equations presented in the *AASHTO Specs*.
- As indicated by the *AASHTO Specs*, a refined method of analysis is necessary to fully analyze the response of the bridge.

Next, regarding the thermal field assessment:
- Axial stresses showed larger ranges than both major axis and flange lateral bending stresses due to expansion and contraction of the bridges.
- With an effective annual temperature range of 100 °F, thermal loads induced

axial girder stresses of up to 6.4 ksi and a total stress of up to 12.0 ksi.

- Thermal stresses accounted for an approximate average of 70% of the total combined loading stress for live loads and thermal loads in the exterior girders.

- The temperature induced stresses were approximately 19% of the yield stress for Grade 60 steel.

- No discernible differences were existed between the horizontally curved bridges and the straight bridge as thermal results were found to be approximately the same throughout all five bridges.

- These results may point out that the support conditions of these types of bridges may play an important role in determining the total stress that must be resisted by the superstructure.

CHAPTER 5 ANALYTICAL INVESTIGATION OF DESIGN LOADS ON HORIZONTALLY CURVED GIRDER BRIDGES WITH INTEGRAL ABUTMENTS

Modified from a paper prepared for submission to ASCE's *Journal of Bridge Engineering*

Jerad J. Hoffman and Brent M. Phares

Abstract

A small degree of uncertainty has been observed for determining the significance of thermal loads when designing the superstructure in a horizontally curved steel bridge. This investigation focuses research on a three-span curved bridge with fixed piers and integral abutments. Combining horizontal curvature with increased levels of fixity presents growing concern with regards to the influence of changing temperatures. The purpose of this work was to analytically investigate the superstructure behavior under design thermal loading conditions. In doing so, a bridge previously subjected to an empirical field study was modeled using a commercial finite element analysis software package. Results indicated that stresses in the lower flange of the girder, due to applied thermal loads, were greatest at the fixed pier locations. These stresses were mostly due to lateral flange bending caused by the pier restraining lateral movement of the girder. While these stresses were small for this particular bridge, adding only up to 3.0 ksi, bridges incorporating integral abutments and fixed piers with increased curvature and skew may require special attention in future practice.

5.1 Introduction

Upon discussions with a major, international design-consulting firm, it was determined that the influence of thermal effects in the superstructure design of bridges has traditionally been neglected depending on certain bridge conditions and the experience of the engineer. However, restraining horizontally curved bridges with increased pier and/ or abutment fixities generates a growing level of uncertainty in the significance of neglecting such thermal effects. A common design practice in straight bridges, based on experienced

engineering judgment, may be to implement conservative design procedures to adequately offset the assumed small stresses generated from thermal loads. To at least some extent, this same practice is exercised for horizontally curved bridges. Due to the seeming level of uncertainty with respect to thermal effects on a complex curved bridge superstructure, an investigation into the matter was initiated.

Previously, an empirical field study was performed to monitor the behavior of a newly constructed horizontally curved bridge, referred to as Bridge 309 hereafter. The readily available results from the field study provided a prime opportunity to further analytically investigate the behavior of the bridge under design load conditions, particularly with regards to live loads and thermal loads.

Structural analysis of a bridge, in accordance to the 2010 AASHTO LRFD Specifications Section 4.5, requires any method to satisfy equilibrium, compatibility, and proper stress-strain relationships for a given material. Examples of such methods include classical, finite difference, finite element modeling (FEM), folded plate, finite strip, yield line, and grillage methods. Often, a horizontally curved girder bridge requires a refined method of analysis.

A refined method of analysis is defined as one that includes the superstructure as an integral system providing adequate displacements and reactions. An engineer may neglect the horizontal curvature component and apply approximate methods of analysis if the geometry meets certain criteria outlined in Article 4.6.2.2.4. These criteria often pertain to limiting bridge skew, maintaining constant cross sections, and limiting radius to arc span length ratios. Approximate methods of analysis require significantly less effort as several assumptions are made throughout the process. Simplifications and assumptions made in the approximate methods greatly reduce time.

Bridge 309 does not meet the criteria established in Article 4.6.2.2.4 of the AASHTO LRFD Specifications. Consequently, a refined analysis method must be employed. Nevling et al. (2006) attempt to evaluate the level of accuracy produced for various analysis methods through conducting research on a continuous three-span bridge. Three levels of analysis were established. Level 1, being the simplest, consisted of simplified empirical methods. Level 2 entailed the use of the 2-D grillage method. Lastly, Level 3, being the most complex, explored the 3-D FEM. Conclusions were made by comparing the three methods of analysis against one another, as well as the methods against field data. Results showed Levels 2 and 3

predicted major axis bending moments most similar to the field results. According to Lydzinski et al. (2008), the FEM method is beneficial for multispan horizontally curved steel girders. Modeling certain details in order to capture structural behaviors cannot be completed any other way. Details such as bracing connections and element type combinations can play an important role when analyzing a complex structure similar to the horizontally curved bridges in this study.

<h2 align="center">5.2 Model Development</h2>

Two general types of elements were used to develop the analytical model of Bridge 309. A 3-D elastic shell element with both bending and membrane capabilities was used when modeling the abutment, deck, and web of the girders. A 3-D uniaxial elastic beam element with tension, compression, torsion, and bending capabilities was used to model the abutment piles, pier caps, pier columns, and girder flanges.

The materials properties used in the model consisted of steel and concrete. Certain assumptions were made for the thermal and structural properties of the concrete and steel in order to simplify the modeling. Values for the modulus of elasticity, Poisson's Ratio, and coefficient of linear thermal expansion were selected based on typical material values.

Boundary conditions varied throughout different stages of the study in order to accomplish specific tasks and comparisons. Reasons for making changes in boundary conditions and of the attributes will be noted as needed.

5.2.1 Bridge Description

Bridge 309, is a 26 ft wide, three span, integral abutment bridge with a 950 ft horizontal baseline curvature radius, and spans of 85 ft, 149 ft, and 85 ft. The abutments and piers are skewed at 15° left ahead. Both piers are fixed (FP) for translation and released for rotation. Both abutments are fully integral abutments (IAB). The bridge has non-composite bent plate diaphragms that are connected to the welded, I-shaped, composite, steel-plate girders. The typical cross section is shown in Figure 5.1 with Girder D located towards the center of curvature. Girders B, C, and D have equal stiffness and Girder A has an approximately 16% higher stiffness.

48
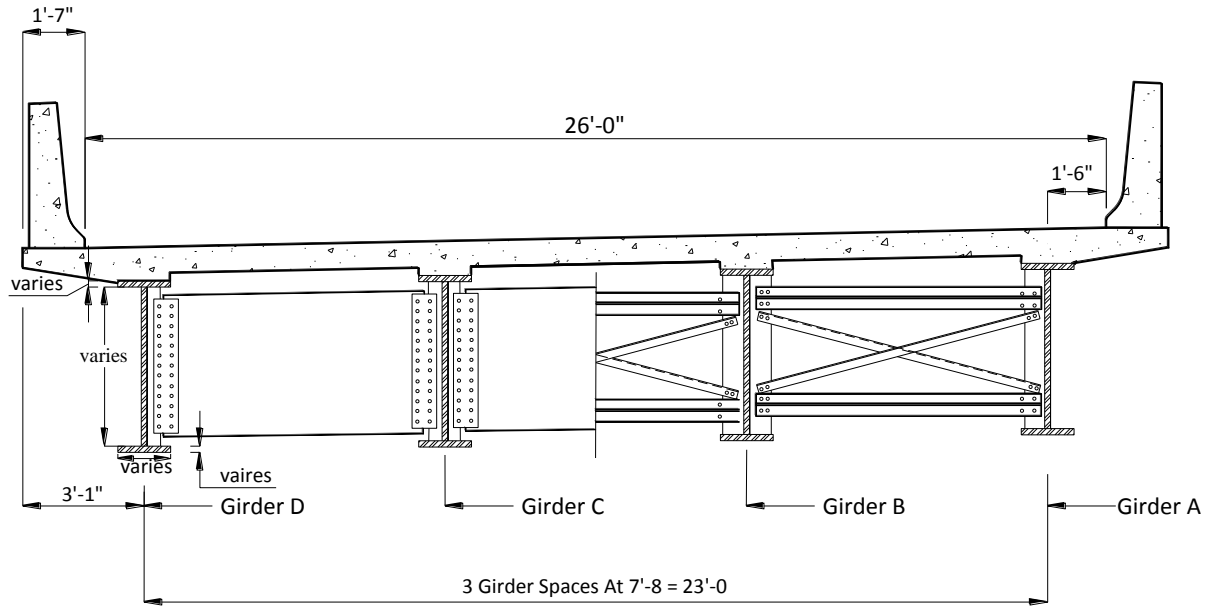
Figure 5.1. Typical bridge cross section

Considering that the girder and diaphragm responses were the main focus of this study, much attention to detail went into establishing respective mesh sizes and connecting them. The diaphragms were modeled by directly attached to the girders along their full depth. Directly attaching these components required that girder elements and diaphragm elements share common nodes in both the girder's web and flanges.

Lydzinski et al. (2008) described that the number of elements per girder cross section has little influence on results. Conversely, the results are more sensitive to a finer mesh with respect to the longitudinal length of the bridge. Lydzinski et al. further suggested that the element length should roughly equal 2% of the span length. As a result, approximate element lengths of were chosen accordingly.

Parapet models were simplified by assuming an average constant thickness and directly attaching them to the deck. The deck was assumed to be a constant 8 in. thick connected to the girders with rigid links to create composite section properties. Live loads – when applied – were applied directly to the deck as point loads.

Pier columns and cap components were modeled as a frame about their centerlines. The pier columns were modeled using tapered members to account for their varying cross sectional area. An illustration of the simplified frame pier geometry can be seen later in Figure 5.2.

Rigid links also connected the bottom of the girders to the center line of the pier caps. The rigid link nodes attached to the pier were restrained for all degrees of freedom (DOFs), while the nodes on the bottom of the girders were released for rotation in the plane tangent to the curvature about the strong axis of the girders. Releasing this rotation accurately represented fixed pier behavior. Piers were assumed to be completely fixed at the base of the modeled columns as the footings were assumed to be rigid.

The abutment model utilized the as-built abutment dimensions. Based upon the work by Abendroth, the abutment piles were modeled using an equivalent cantilever length of 18 ft (Abendroth et al. 2005). Both abutments were directly attached to the girders, deck, and abutment piles (Figure 5.2).

The abutment piles provide the rotational restraint provided by an integral abutment. The effective cantilevered piles were oriented such that their weak axis coincided with the abutment centerline. All rotation and translation degrees of freedom (DOF) were restrained at the base of the piles to represent the effective cantilever.

In this work two basic models were considered. The "field" model considered all of the elements in the as-built bridge as described above. A second model known as the "consultant" model was developed to compare with a more traditional design/ analysis approach. The consultant's design model substituted simple supports for the substructure components mentioned above. Additionally, the parapets were excluded in the consultant model as they are not considered in design practice.

Boundary conditions were applied directly at nodes in the bottom of the girder ends, where the abutments and piers would be located. DOFs at these nodes were fixed for translation and released for the girder rotation. These supports at the abutments represented classical pinned support condition. Supports at the piers were idealized as rollers, releasing the translational DOF in the girder's y-axis direction and the rotational DOF about the girder's x-axis.

5.2.2 Model Validation

Model validation will be achieved by comparing the analytical results to two separate data sets. First, the model will be tailored to compare with the experimental results, referred to as "field" hereafter. Additionally, the model will be tailored to compare results provided

from a consulting design firm, referred to as "consultant" hereafter. Upon validation of this study's analytical model, further exploration of design loading effects will be presented.

5.2.3 Field Live Load Validation

For a separate field study on the live load behavior of curved integral abutment bridges, the superstructure of the subject bridge was instrumented with 40 strain transducers. Each of the four I-girders was outfitted with four transducers at two separate radial cross-sections located in the northern end span. The first cross section, Section 1, was located at half the unbraced length between two diaphragms. Section 2 was located where diaphragms are present. Both sections are parallel to the radius of curvature and adjacent to one another.

Live load testing was conducted for a load placed at three load paths. Load Path 1 (LP1) located towards the inside of the curve, Load Path 2 (LP2) centered on the bridge deck, and Load Path 3 (LP3) located towards the outside of the curve. For each path, the truck traveled across the bridge along the individual load path at a walking pace.

Live loading was applied to the model according to the truck dimensions, axle weights, and transverse axle locations from the field testing. Prior to processing data, deflected shapes of the model were verified at various truck positions. Figure 5.2 shows the deflected shape for a truck positioned in the first span for the outer load path. Note that the plotted deflections are not to scale.
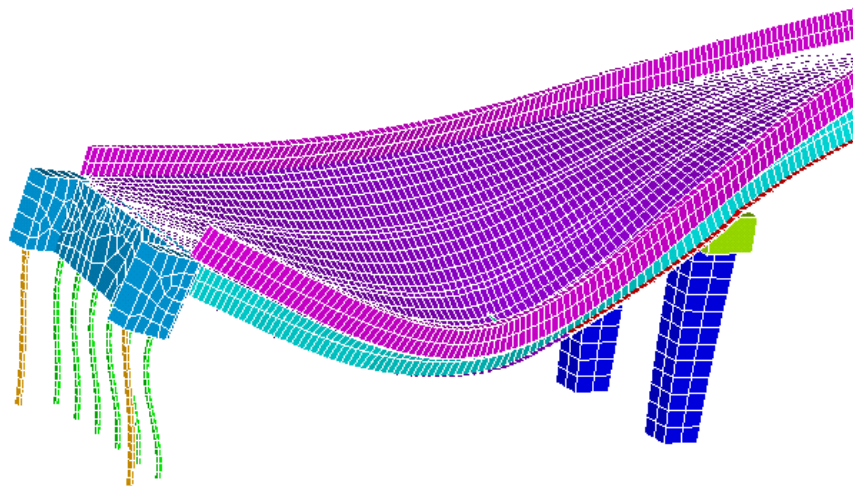
Figure 5.2. Deflected shape for outer truck position in first span

Once several deflected shapes were plotted and reviewed, the girder strains were

extracted at bridge Sections 1 and 2. The analytical strains were then directly compared to the strains from the study.

While comparing strains, girder bottom flange strains were of specific interest due to their large magnitudes relative to the top flange strains. Figure 5.3 displays a typical comparison between analytical and field results.
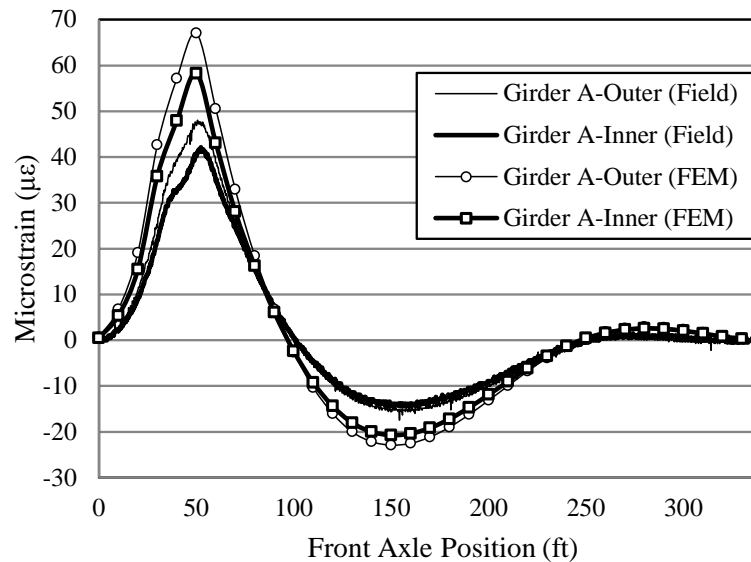
Figure 5.3. Typical Analytical vs. Field bottom flange strain comparison

The comparisons, typically shown in Figure 5.3, indicate that the analytical model predicted larger bottom flange strains at all girder locations for all load paths. Upon summing the peak bottom flange strains of all girders at a given bridge section, the results produced differences ranging from 12% to 22%. The magnitude of difference was least when the truck was centered and near Section 1. Since Section 1 is located between two diaphragm sets, results may indicate that the behavior of the modeled girder-diaphragm interaction diverges from the actual field condition.

Another key behavior is also shown in Figure 5.4. The analytical model corroborated the field results with respect to outer and inner flange tip strain variations. Results from the modeling showed that the outer and inner flange tips vary in strain magnitudes. This trend validates that the analytical model not only predicted lateral bottom flange bending behavior that is present in horizontally curved girders, but also correctly predicted the direction of lateral flange bending as shown from field testing. Figure 5.4, viewed from the bottom of the

superstructure, plots the laterally deflected girders for a centered truck in the first span of Bridge 309. It was concluded analytical values match experimental field tests reasonably well and the analytical model validation is considered acceptable with respect to the field live load response.
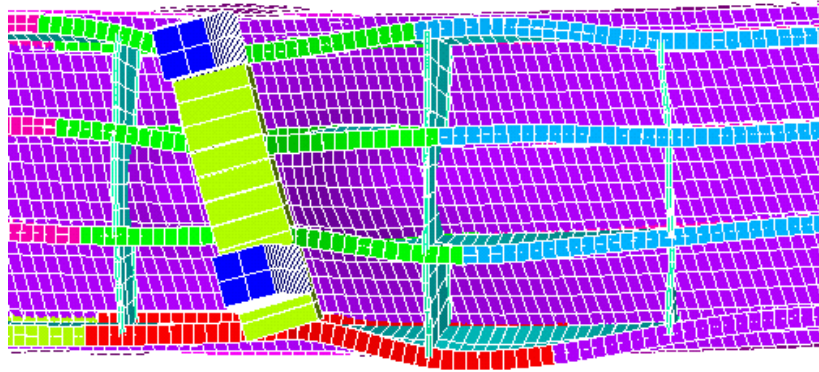
Figure 5.4. Laterally deflected girders

5.2.4 Field Thermal Validation

In a previous field study, bridge responses under different temperatures were measured. The temperature behavior was similarly assessed with the analytical model by applying a uniform increase in temperature. For the steel, ΔT_s equal to 80^0 F; and for the concrete, ΔT_c equal to 50^0 F. Results produced an axial strain equal to -129 $\mu\varepsilon$ in Girder A at Section 1 of Bridge 309. Referring to Equation 5.1, and applying appropriate material properties, the applied temperatures represent an effective bridge temperature, ΔT_{eff}, equal to 63.5^0 F for use in the analytical analysis.

$$\Delta T_{eff} = \frac{(A_c E_c \alpha_c \Delta T_c + A_s E_s \alpha_s \Delta T_s)}{(A_c E_c \alpha_c + A_s E_s \alpha_s)} \quad (5.1)$$

From the thermal field results, an axial strain range of 170 $\mu\varepsilon$ *was measured with an effective bridge temperature of 100^0 F. Proportionally increasing ΔT_{eff} in the model from* 63.5^0 F to 100^0 F would produce an analytical axial strain equal to -200 $\mu\varepsilon$ *in Girder A.* Thus, the comparison of the thermal field study to the thermal analytical model validates, in a very simple and generic manner, the thermal analysis results.

5.2.5 Comparison with Consultant Model

Once the geometric model modifications mentioned previously were made, live loading was then applied in similar fashion to the field study model for both the analytical and consultant models. For simplicity, only the center and outside load paths were considered. In post-processing, deflected shapes of the model were verified at various truck positions. All deflected shapes for the live load positions agreed with the assumed overall structural behavior of the bridge.

Next, the analytical model output was compared to the supplied output from the consultant design model. The consultant presented results in terms of strong axis bending moments and lateral bottom flange bending moments. Thus, the validation compared calculated moments at Sections 1 and 2 for LP2 and LP3. Each of the four girders was directly compared to the consultant's results. Figure 5.5 represents typical comparisons to lateral flange bending moments and strong axis bending moments for Girder A.
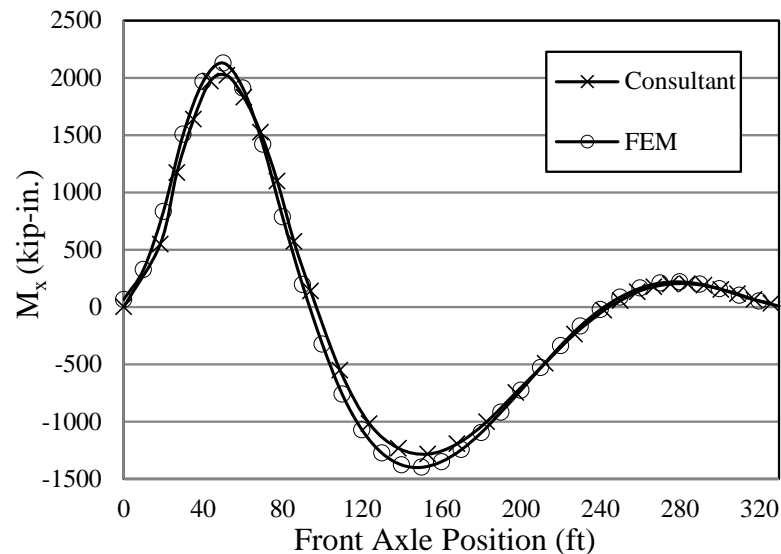
Figure 5.5. Girder A: Center Path at Bridge Section 1

Strong axis moments differed between the analytical model and consultant by an average 6.0% at peak truck locations in all girder sections. Furthermore, lateral bottom flange moments differed by less than 4.0 kip-in at peak truck locations in all girder sections. As a result, the analytical model developed for this work was considered to compare well with the consultant's design model.

5.2.6 Design Loads and Combinations

With the analytical model validation complete, the study then investigated design loading conditions. The loading conditions selected were based on the design limit states in accordance with the AASHTO LRFD Specifications. For the scope of this study, the Strength I and Service I load combinations from Table 3.4.1-1 in the AASHTO LRFD Specifications were assumed to govern the design. These load combinations included components for dead load, live load, water load, thermal load, wind load, settlement, and friction load. However, for the scope of this study, only the dead, live, and thermal loads were considered. In reference to Table 3.4.1-1, Equations 5.2 and 5.3 represent the load combinations considered throughout the remaining discussion of this work.

$$\text{Strength I} = \gamma_p DC + 1.75 LL(1+IM/100) + \gamma_{TU} TU + \gamma_{TG} TG \quad\quad (5.2)$$

$$\text{Service I} = 1.00 DC + 1.00 LL(1+IM/100) + \gamma_{TU} TU + \gamma_{TG} TG \quad\quad (5.3)$$

Dead Load

Dead loads from the structural components, DC, included the weights of the deck, steel girders, steel diaphragms, and parapets. Assumed material densities were assigned to the proper structural components in the model. Maximum and minimum load factors, γ_p, of 1.25 and 0.90 were applied for the Strength I load combination. The minimum load factor was used when the force results from the live load were not additive to the dead load results.

Live Load

Vehicular live loading, LL, was the HL-93 load, consisting of the combination of a design truck or design tandem, and the design lane load. The combination of the design truck and the design lane load were assumed to govern for this work. Design lanes are 12.0 ft wide and the number of design lanes is based on the roadway width. Bridge 309 has a 26.0 ft roadway width, so the number of design lanes equals two.

The 0.64 klf uniformly distributed design lane load occupies a 10.0 ft transverse width within the design lane. The load was distributed over the entire length of the bridge and superimposed on top of the design truck load. For the scope of this study, the 14.0 ft axle spacing was assumed to control. Since Bridge 309 has two design lanes, two design trucks were placed side by side along the bridge's centerline. Placing the truck's side by side would

produce maximum responses to live load.

Load factors for Strength I and Service I load combinations were taken as 1.75 and 1.00, respectively. A vehicular dynamic load allowance, IM, of 33% was applied to the static live load application for both load combinations. Note that only the design truck is subject to the IM.

Thermal Load

Design loads also considered two thermal loads, a uniform temperature and a temperature gradient. A uniform temperature was applied to the entire depth of the superstructure. Procedure A from Section 3.12.2.1 in AASHTO LRFD was used to determine the maximum and minimum temperatures for the model. Temperature ranges are based on the classification of the bridge due to material type and location. Bridge 309 classifies as a steel or aluminum structure located in a cold climate.

The thermal analysis assumed two lock-in temperatures for a positive (+TU) and negative (-TU) temperature change. Lock-in temperatures were based on acceptable temperatures for placing concrete during construction. By choosing the upper and lower bounds for acceptable pouring temperatures, the positive and negative uniform temperatures changes could then be chosen accordingly. For a positive uniform temperature change, the lock-in temperature was assumed to be 40°F; yielding +TU equal to 80°F to reach the upper temperature range of 120°F. For a negative uniform temperature change, the lock in temperature was assumed to be 80°F; yielding -TU equal to -110°F to reach the lower range of -30°F.

The temperature gradient, TG, applies three temperatures throughout the depth of the superstructure in addition to the uniform temperature values. Temperature 1 (T_1), at the top of the deck, and temperature 2 (T_2), in the middle of the deck, for the positive temperature gradient, were selected based on the geographic bridge location in Section 3.12.3 in the *AASHTO LRFD Specifications*. Temperature 3 (T_3) was constant for the depth of the girder. T_1 equals 46^{0}F, T_2 equals 12^{0}F, and T_3 equals 8^{0}F. Negative temperature gradient values were obtained by multiplying the positive values by -0.30 for plain concrete decks with no asphalt overlay.

5.3 Results and Observations

In order to focus the exploration of the design loading conditions, the study focused on

results near approximate maximum positive and maximum negative moment regions. Strains were extracted for each of the four girders at seven cross sections along Bridge 309. The seven cross sections consisted of three mid-span cross sections representing positive moment regions and four support cross sections for negative moment regions. The sections located at mid-span are parallel to the bridge radius while the sections near supports are parallel to the bridge skew.

5.3.1 Preliminary Results

A preliminary review of results indicated that typical trends could be characterized by two of the seven cross sections. The Center Span cross section represented girder behavior for maximum positive moment regions. The cross section at the North Pier represented girder behavior for maximum negative moment regions. Initial results concentrated on relative magnitudes of strong axis bending, lateral bending in the bottom flange, and axial forces for each loading condition.

Girder A, the outside girder, typically produced the maximum results at the Center Span and North Pier cross sections. Table 5.1 and Table 5.2 tabulate the unfactored internal forces of strong axis bending moment, M_x; lateral bottom flange bending moment, M_{lb}; and axial force, P; for each of the design loads in Girder A.

Table 5.1. Girder A: Unfactored internal forces at North Pier

N. Pier	DL	LL	T(+)	T(-)
M_x (kip-ft)	-1730	-745	98.4	-172
M_{lb} (kip-ft)	8.9	5.7	-23.3	31.0
P (kip)	24.0	10.7	-150.2	328

Table 5.2. Girder A: Unfactored internal forces at Center Span

C. Span	DL	LL	T(+)	T(-)
M_x (kip-ft)	1480	1030	-78.4	150
M_{lb} (kip-ft)	-6.0	-4.7	1.2	-2.4
P (kip)	-72.2	-53.3	-70.2	224

Note that live load results were recorded from peak truck positions for each respective cross section. Also, thermal results were separated into positive and negative temperature changes. Each temperature change combined both the uniform and gradient temperatures, previously specified.

Influences of thermal loadings proved to be present upon further assessment of Table 5.1 and Table 5.2. A negative temperature change produced a strong axis moment nearly one-quarter of the moment due to live loading at the North Pier. Furthermore, lateral flange moments were over six times greater than the lateral flange moments produced by the live load. Finally, maximum thermal axial loads were significantly greater than that of dead and live load results for all girder cross sections.

Even though the contributions of temperature are to be included in Strength I and Service I limit states according to AASHTO LRFD, bridge designers frequently neglect the influences of thermal loadings. Conservative assumptions are made based on boundary conditions and degrees of fixity within the structure to offset the possible internal thermal forces. Increased efforts and uncertainty in thermal analysis tends to lead designers away from assessing thermal loads because their influence is assumed insignificant. Regarding superstructure design, temperatures are only taken into account in extreme design cases, deemed necessary by designer or owner. However, since the above tables suggest that thermal loads may have contributions to design load conditions, the study further investigated the matter. The proceeding figures in this chapter help determine the significance of including thermal loading and/ or modeling substructure entities.

To determine the significance, two different models will be compared in this section. This study attempted to decide whether that assumption is appropriate by comparing the load effects for the simply supported model, referred to as the "Simple" model, versus the model that included the abutments and piers, referred to as the "Full" model. In summary, the models are as follows:

- Full model: includes abutments, piers, and applies thermal, dead, and live loads (results represented by solid lines in accompanying figures)
- Simple model: assumes simple supports and applies only dead and live loads (results represented by dashed lines in accompanying figures)

5.3.2 Service I Load Conditions

Strong Axis Bending

Girder responses to individual Service I load conditions were calculated for all four girders at the North Pier and Center Span cross sections. Service I strong axis moments due to thermal loads proved to be noticeable but less influential compared to dead and live load moments. Thermal strong axis moments contributed a maximum of 9% to the total negative moment at the North Pier in Girder C. Temperature had an even less significant influence at Center Span where the maximum contribution to the total moment is 6%.

Replacing substructure entities with the simply supported model produced negligible differences in results. Less than a 3% increase in strong axis moments (Center Span) due to dead load and live load were present. This slight increase may suggest the simply supported conditions do not increase results due to dead and live load as sometimes assumed.

Lateral Bottom Flange Bending

Results indicate that thermal lateral bending moments in the bottom flanges ranged from -57 kip-ft to 43 kip-ft at the North Pier. Lateral bending moments in the bottom flanges for thermal loads were greater than dead or live loads in Girders A, B, and D at the North Pier. The exterior two girders, A and D, had the largest responses to temperature. After combining dead, live, and thermal lateral moments in Girder D, a positive temperature increase contributed to nearly 50% of the sum. Conversely, thermal lateral bending moments were rather insignificant at Center Span.

Replacing the substructure entities with simply supported conditions yielded smaller lateral bending moments in the bottom flanges for dead and live load conditions. The simply supported assumption proves to be unconservative with respect to lateral bending in the bottom flange, particularly at the pier.

Based on simple mechanics of materials, an undeformed curved member subjected to a constant increase in temperature will uniformly increase in overall length and radius of curvature. Support conditions similar to the piers and abutments in Bridge 309 will restrain such translational movement. Thus, the piers hinder the uniform deformation of the member, especially the lower flange which is connected directly to the pier. Restraining the deformation of the horizontally curved member increased lateral bending, particularly in the bottom flange, at the fixed pier location. The development of the results presented in Table

5.1 and Table 5.2 call special attention to lateral bottom flange bending due to temperature changes at fixed pier locations.

Axial Forces

Axial forces due to thermal loads were found to be much greater compared to the dead and live load conditions at both the North Pier and Center Span. Temperature changes produced average girder axial forces ranging from -217 to 358 kips and -195 to 326 kips at the North Pier and Center Span, respectively. The axial forces produced at the North Pier due to dead and live loads are small in comparison to the thermal results. At the Center Span, girder axial forces due to combined dead and live loads had a greater influence with an average of -141 kips.

Incorporating simply supported conditions had little effect on axial forces at the North Pier due to the negligible results produced from dead and live loads. However at the Center Span, girder axial forces from the simply supported model produced an average -67 kips due to combined dead and live load. Only 48% of the axial forces produced by incorporating the substructure model were present in the Simple model. Again, the assumption of replacing substructure entities with simply supported conditions proves to be unconservative with respect to axial forces produced from design loads in the superstructure.

Summary

According to the results presented thus far, temperature appeared to influence the substructure behavior for Service I level loading conditions. Axial loads due to temperature produced the most significant results as they often accounted for most of the total force at all cross sections along the bridge. Lateral bending moments in the bottom flange proved to be most influential for temperature changes at fixed pier locations, accounting for up to 50% of the total lateral moment in bottom flanges. Strong axis bending moments due to temperature were less influential; however, their presence was still noticeable as they contributed up to 9% of the total moment in the composite section. Lastly, removing substructure entities and replacing boundary conditions with the simply supported model proved to be unconservative for the axial forces and lateral bottom flange bending moments.
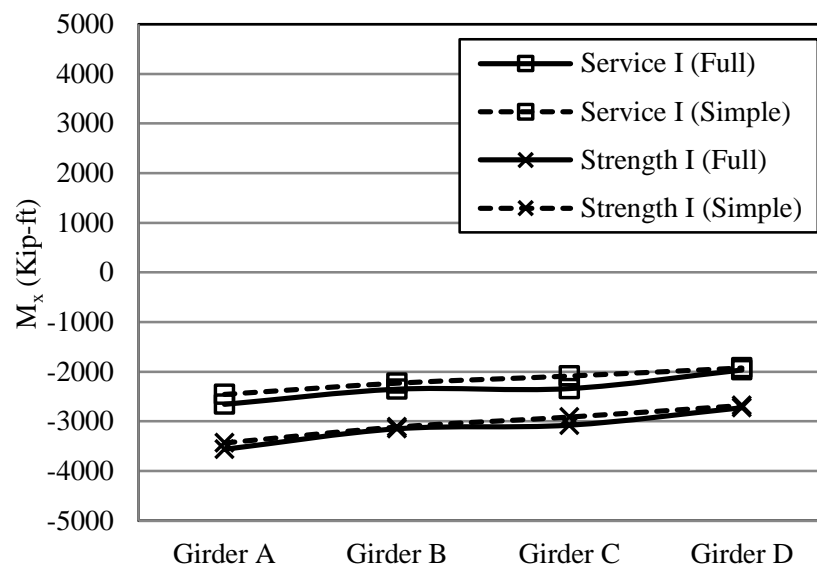
5.3.3 Load Combinations

Service I level results further suggest that thermal loads may be critical in the design of

Bridge 309. However, Strength I load conditions often govern the design of girder members. The accompanying results of this subsection attempt to show whether or not the Strength I load factors minimize the effect of the increased temperature forces while including substructure entities.

Strong Axis Bending

Figure 5.6 plots the combinations of Strength I and Service I strong axis moments in the composite section at the North Pier. As noted, a thermal analysis was conducted for both negative and positive temperature changes. The load combinations account for only the thermal analysis that yielded the critical loading combination. In other words, the thermal load results were to be additive to the dead and live load results. The solid lines represent the model that includes the substructure entities and accounts for the thermal loads, referred to as the "Full" model. The dashed lines represent the simply supported model that does not include thermal loads, referred to as "Simple" in the associated figures.
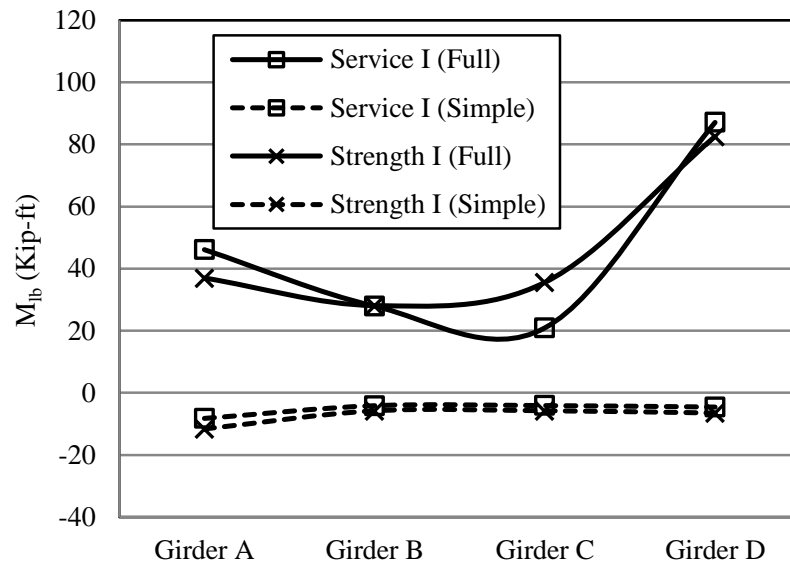

Figure 5.6. North Pier: Load Combinations

Results in Figure 5.6 show that strong axis moment magnitudes were up to 5.6% more for the Strength I Full model at the North Pier compared to the Simple model. Overall, including the substructure and incorporating thermal loads in the analysis provide only slight variances with regards to strong axis composite section moments.

Lateral Bottom Flange Bending

Figure 5.7 plots the combined loads for the lateral bottom flange bending moments. Again, including thermal loads and substructure entities yield the largest lateral moments. The impact of temperature loads in the Full model is most profound at the fixed pier location. Lateral flange bending moments at the Center Span are negligible for all loading conditions when compared to the pier locations. Service I produced slightly larger lateral moments in the exterior girder's flanges while Strength I produced larger lateral moments in the interior girders. Because the relatively large lateral bottom flange moments are not present in the Simple model, the Full model exemplifies the unique behavior a curved member exhibits from thermal loads at restrained support locations.

Figure 5.7. North Pier: Load Combinations

Axial Forces

Figure 5.8 plots the Service I and Strength I axial load combinations. Service I produced the largest axial forces in all four girders at the North Pier and in only Girders A and C at the Center Span. More importantly, inclusion of the substructure model and thermal effects yielded axial load magnitudes up to 12 times greater than the Simple model. This large increase emphasizes the significance of a thermal analysis for determining axial loads.
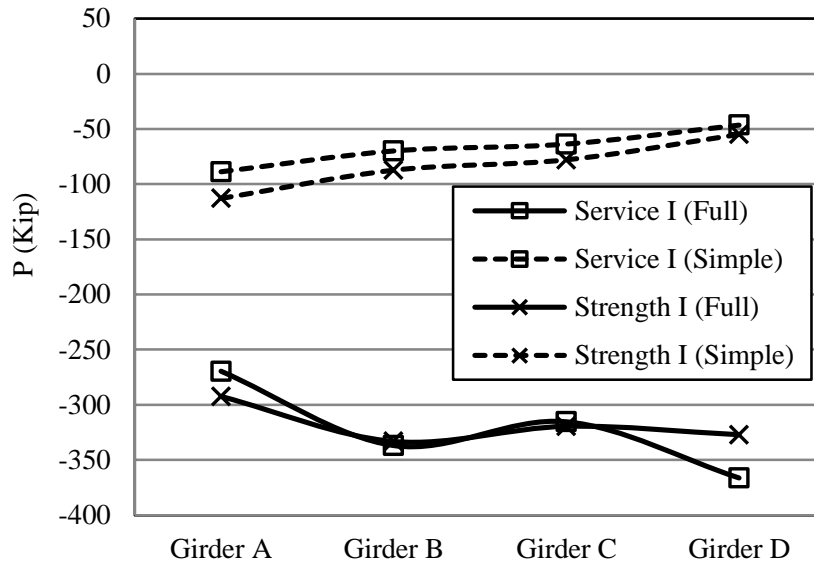
Figure 5.8. Center Span: Load Combinations

Stresses

Observations from the previous results indicate that both the Strength I and Service I load combinations are dependent on including a thermal analysis to assess strong axis moments, lateral bottom flange moments, and axial forces in a girder section. Even though the internal moments and forces produced from temperature changes are noteworthy, it was deemed necessary to study the effects temperature has on the stress levels. So, for example, even though the relative effect of temperature on bottom flange bending moment may be large, the effect of the bottom flange bending stress may be small relative to the major axis bending stresses produced from dead and live load.

Table 5.3 and Table 5.4 tabulate the Strength I design load stresses at the North Pier and Center Span cross sections from the Full model. Results are in terms of internal components consisting of strong axis bending stress, σ_x; lateral bottom flange bending stress, σ_{lb}; and axial stress, σ_a. Additionally, the last four rows in Table 5.3 and Table 5.4 provide the total individual girder stress, $\Sigma\sigma_{total}$, for each loading case as well as the stresses from combined loading.

Table 5.3. North Pier: Strength I Stresses

	Girder	DL	LL	T(+)	Combined Loads
σ_x (ksi)	A	-10.2	-6.1	0.3	*-16.0*
	B	-11.0	-6.4	-0.2	*-17.5*
	C	-10.2	-6.0	-0.5	*-16.7*
	D	-9.4	-5.4	-0.1	*-14.8*
σ_{lb} (ksi)	A	-0.9	-0.8	-0.9	*-2.6*
	B	-1.1	-1.0	-0.5	*-2.6*
	C	-2.1	-1.7	-0.2	*-4.0*
	D	-3.5	-2.7	-2.0	*-8.2*
σ_a (ksi)	A	0.2	0.1	-0.8	*-0.5*
	B	-0.1	0.1	-0.9	*-0.9*
	C	-0.2	-0.1	-0.8	*-1.1*
	D	0.1	0.3	-0.7	*-0.4*
$\Sigma\sigma_{total}$ *(ksi)*	A	*-10.9*	*-6.8*	*-1.4*	***-19.0***
	B	*-12.1*	*-7.3*	*-1.6*	***-21.1***
	C	*-12.4*	*-7.8*	*-1.5*	***-21.7***
	D	*-12.8*	*-7.8*	*-2.7*	***-23.3***

Table 5.4. Center Span: Strength I Stresses

	Girder	DL	LL	T(-)	Combined Loads
σ_x (ksi)	A	12.4	12.1	0.5	*25.1*
	B	11.9	11.9	0.3	*24.0*
	C	11.3	11.4	0.3	*22.9*
	D	10.6	10.8	0.0	*21.4*
σ_{lb} (ksi)	A	0.8	0.9	0.2	*1.9*
	B	0.9	1.0	0.2	*2.0*
	C	0.9	0.9	0.2	*2.0*
	D	0.9	1.0	0.2	*2.0*
σ_a (ksi)	A	-0.6	-0.6	1.0	*-0.2*
	B	-0.7	-0.7	1.2	*-0.1*
	C	-0.7	-0.7	1.2	*-0.2*
	D	-0.5	-0.6	1.5	*0.4*
$\Sigma\sigma_{total}$ *(ksi)*	A	*12.7*	*12.4*	*1.7*	**26.8**
	B	*12.1*	*12.1*	*1.7*	**25.9**
	C	*11.5*	*11.6*	*1.6*	**24.7**
	D	*11.0*	*11.1*	*1.6*	**23.8**

As previously stated, the stresses presented in Table 5.3 and Table 5.4 represent only a small portion of the total design stresses that are considered in practice. The purpose of this portion of the study is to merely evaluate the effect that temperature changes may have on a horizontally curved steel I-girders. In doing so, the dead and live load results provide references to assess the magnitudes of the thermal results.

Notice that Table 5.3 and Table 5.4 only provide results for one thermal load case, T(+) or T(-). The controlling thermal load at the individual section was selected based on the critical total stress produced in the section. An increase in temperature, T(+), was found to be the controlling thermal case at the North Pier; while on the other hand, a negative temperature change, T(-), controlled the thermal loading at the Center Span.

The tabulated results indicate that the strong axis bending stresses contribute most to the total stress (for DL and LL). Strong axis bending from combined loading accounts for an average 92% and 77% of the total stress from combined loading at the Center Span and North Pier, respectively. Thermal loads contribute only up to 3% of the combined strong axis

bending stress in Girder C at the North Pier.

Contrarily, thermal loads had more influence at the fixed pier location for lateral bottom flange bending. In the most extreme case of Girder D, lateral bending stresses in the bottom flanges were greatest at the North Pier. After applying Strength I load factors, combined loading produced a lateral bottom flange bending stress magnitude of 8.2 ksi. Thermal loads produced maximum lateral flange bending stresses of 2.0 ksi. Though this quantity is less than the lateral stress produced from the dead and live load of 3.5 ksi and 2.7 ksi, respectively, the thermal contribution to the stress in the flange may be significant to account for in design. At the Center Span, lateral bending stresses were less at only 2.0 ksi, due to combined loading.

Recall that significantly higher axial loads were present due to the temperature changes. However, the constant axial force was found to be relatively small for the size of the composite cross sectional area. Therefore, the stresses yielded less influential results. The maximum axial stress equaled -1.1 ksi, in compression, for Girder C at the North Pier due to combined loading. Thermal axial stress accounted for -0.8 ksi of the total -1.1 ksi, indicating that temperature does indeed account for most of the axial effects. However, axial loads only contribute minimal stresses to the section.

After summing the stresses in individual girders for each load case, thermal loads contribute average magnitudes of 1.8 ksi and 1.7 ksi to the total combined stress for the North Pier and Center Span, respectively. As a reference, for Grade 50 steel, 1.8 ksi correlates to only 4% of the yield stress. As mentioned, the maximum case existed in Girder D at the North Pier. Thermal loads produced a total stress magnitude of 2.7 ksi, or 5% of the yield stress. Thus, concluding that thermal stresses for this curved bridge are small and may only add up to near 3 ksi.

5.4 Conclusion

During the investigation of thermal loading conditions detailed by the 2010 AASHTO LRFD Specifications, significant results were observed that could impact the approach for designing and analyzing the superstructure of horizontally curved steel I-girder bridges with integral abutments. The following statements summarize the conclusions found within this research.

- Strength I axial forces were nearly three times larger for thermal loads than dead and live loads as caused by expansion and contraction along the length of the bridge.

- Special attention has been drawn to the increased lateral bottom flange bending at fixed pier locations as Strength I lateral bottom flange bending moments were nearly ten times greater when including temperature effects.

- The significant thermal effects indicate that including thermal loads is essential in order to fully assess the magnitudes of the girder forces.

- The Strength I thermal loads may produce up to 3.0 ksi of stress in the bottom flange of the girder for bridges with similar geometry to those that were researched in this work.

- Increasing degrees of skew, curvature, and levels of restraint, particularly in the bottom flange at fixed pier locations, may increase these thermal induced forces even more; thus, more noteworthy stresses could be produced in the flanges of the girder due to temperature changes.

- A sensitivity analysis is recommended for future work to determine the magnitudes of increased thermal stresses with respect to increased curvature in similar bridges.

CHAPTER 6 GENERAL CONCLUSIONS

The contents of this chapter are separated into the two journal paper topics, presented in Chapters 4 and 5, regarding experimental field studies and analytical investigations. A summary of the research procedures, a discussion of the results found, and the conclusions associated with each paper are summarized within. Recommendations for future design practices and/ or continued research regarding these curved bridges are also included.

6.1 Short and Long Term Experimental Study

6.1.1 Summary of Procedure

The development of the NEMM provided the opportunity to assess the behavior of five, three-span, steel I-girder bridges designed with varying curvature, skew, and support conditions. The bridges at the NEMM were typically instrumented with strain gauges at mid-span of the exterior girders for long term monitoring. Each girder was monitored for approximately 15 months with four gauges located on the upper and lower flanges. In addition to the strain, ambient air and steel temperatures were recorded. Also, internal concrete temperatures were measured with temperature gauges placed at mid-depth of the deck.

In addition to the long term monitoring, the bridges at the NEMM were selected to be live load tested. A truck load was applied using three pre-defined parallel load paths. Monitoring the response of each bridge due to the various truck positions was prepared by instrumenting the girders and diaphragms of the bridge superstructures. In all, each curved bridge was equipped with 40 strain transducers at two radial cross sections and the one straight bridge was equipped with 16 strain transducers at a single cross section. Four strain transducers were placed on both the top and bottom flanges of each girder at the instrumented cross section.

6.1.2 Summary of Results

Short Term

Experimental results produced the largest MDF's in Girder A (the outermost exterior girder) for the bridges with the most severe curvature, Bridges 309 and 2308, with values of 0.57 and 0.63, respectively. For the interior girders, Girders B and C, values ranged from

0.51 to 0.52. The innermost exterior girder, Girder D, ranged from 0.44 to 0.46. For Bridges 2208 and 209, the two exterior girders ranged from 0.44 in Girder D to 0.53 in Girder A. Calculating MDF's for Bridge 309 using the approximate method of analysis in AASHTO produced MDF's equal to 0.58 in both exterior girders and 0.62 in both interior girders for multi-lane loading.

The experimental ratio of M_{lb}/M_x for each girder produced average results ranging from 0.8% to 1.1% for the four curved bridges at a diaphragm section. Based on bridge geometry, the V-Load equation produced ratios ranging from 0.6% to 0.8%. Experimental values for Bridges 309 and 2308 compared well with the V-Load equation results, while experimental values for Bridges 209 and 2208 were larger than the V-Load equation results.

Long Term

The average axial-stress range, σ_a, at measured locations for all five bridges was equal 4.4 ksi. The strong-axis-bending stress range, σ_x, was measured with an average value of 2.1 ksi. The lateral-bending stress range for the top and bottom flanges had average values equal to 0.9 ksi and 0.6 ksi, respectively.

The most extreme case of thermal induced stress was found in Girder D at the center span. An effective temperature range of 100 °F produced a maximum of 6.4 ksi of axial stress. By superimposing the four calculated internal stresses at either the bottom or top flange of the girder, a maximum of 11.6 ksi was produced.

6.1.3 Conclusions and Recommendations

Short Term

Based on the results from the live load field testing and assessment, it was concluded that live load moment distribution factors were primarily influenced by the degree of curvature. The largest MDFs were found in Girder A for the two bridges with the most severe curvature, Bridges 309 and 2308. The MDFs for Girder A in Bridges 2208 and 209, which have less severe curvature, were in between the results for the straight bridge and the results for the two bridges with more severe curvature. Furthermore, the live load field testing results found that the V-Load equation provided a reasonable preliminary estimate of M_{lb} based on the magnitude of M_x and the degree of curvature in the girder near a diaphragm. However, as skew increases in the bridges, the V-Load equation notably under-predicted the

experimental magnitudes of M_{lb}. Consequently, a refined method of analysis would be necessary to fully comprehend the responses of these bridges.

Long Term

The internal axial stress results exhibited the largest ranges of all four stress components when considering bridge behavior under thermal loading. For the most extreme case in Girder D at center span in Bridge 2308, an axial stress may equal up to 6.4 ksi. After superimposing all four stress components in this girder, the stresses approached 11.6 ksi. When compared to the live load stresses, the thermal stresses accounted for an average of 70% of the total combined loading stress, or approximately 19% of yield stress for Grade 60 steel. These thermal induces girder stresses, which do not account for other load conditions, were relatively equal in all five bridges. As a result, no apparent differences were discovered when comparing the curved bridges to the straight bridge with respect to the experimentally collected data relating to thermal induced stresses. However, these results indicate that support conditions in these bridges may be significant when considering the total stress in the girders during design.

6.2 Analytical Investigation

6.2.1 Summary of Procedure

A single bridge of the empirical field study at the NEMM was subject to further analytical study. In doing so, a finite element static analysis was performed to investigate the superstructure behavior under design loading conditions, particularly design thermal loads. Bridge 309 was selected as the focus of the investigation because it had the most severe curvature, greatest level of restraints, and it was equipped with the most amount of field instrumentation. The analytical finite element model used a combination of 3-D beam and 3-D shell elements to model key superstructure and substructure entities. Once the model was completed, results from the empirical field study were used to validate the model and increase the confidence of the analytical output. Finally, design loading conditions were applied to the analytical model in order to complete the investigation.

6.2.2 Summary of Results

FEM Validation

Girder strains were used as a basis for comparison with the measured field results. For the live load comparison, after summing the peak bottom flange strains of all girders at a given bridge section, the FEM produced strains 12% to 22% larger than the live load field results. Next, the FEM was compared with the thermal field results through proportioning effective bridge temperatures. Axial strains were approximately 18% larger in the outside girder, Girder A, for the FEM versus thermal field results comparison. Lastly, computed girder forces in the FEM were compared with the provided consultant FEM results. The FEM in this study produced strong axis moments that differed by an average 6.0% and lateral bottom flange bending moments that differed by less than 4.0 kip- in. at peak truck locations in all girder sections when compared to the consultant's results.

Strong axis bending

Strength I load conditions governed over Service I load conditions, producing larger strong axis bending moments by up to 43%. When comparing the Full model to the Simple model, Strength I strong axis bending moments were 5.6% greater for the Full model at the North Pier.

With regards to girder stresses, Strength I strong axis bending due to DL and LL contributed most to the total stress in the bottom flange. At the Center Span, the DL and LL accounted for 92% of the total stress in the bottom flange. The addition of thermal loads contributed only 3% more stress to the combined strong axis bending stress in a single girder.

Lateral bottom flange bending

Lateral bottom flange bending was most profound in the Full model at the fixed North Pier as moments approached 90 kip-ft. Service I produced slightly larger lateral moments in the exterior girders' flanges while Strength I produced larger lateral moments in the interior girders. The simple model produced negligible lateral bottom flange bending results at both the Center Span and North Pier as moments were less than 20 kip-ft.

Considering that Strength I load combinations produced such dominate strong axis bending moments in the Full model, only the Strength I lateral bottom flange bending stresses were calculated. At the North Pier, lateral bottom flange bending produced stresses

up to 2.0 ksi due to thermal loads alone.

Axial forces

Axial forces were much greater in the Full model compared to the Simple model along the entire length of the bridge. Service I produced the largest axial forces at Center Span and similar forces to Strength I at the North Span. Despite the large axial forces, axial stresses were deemed less significant. Thermal axial stresses were less than or equal to 1.5 ksi in each girder at both sections.

6.2.3 Conclusions and Recommendations

Based on analytical analysis results, Strength I lateral bottom flange bending moments were nearly ten times greater when including temperature effects at the fixed pier. Moreover, Strength I axial forces were nearly three times greater when accounting for temperature effects compared to only DL and LL. These results indicate that temperature is an essential consideration when addressing member forces in curved steel I-girders.

With regards to stresses, thermal induced stresses in horizontally curved steel I-girder bridges similar to Bridge 309, with radii greater than 950 ft, are small. Thermal stresses may only add an additional stress of up to 3 ksi in the bottom flange. However, special attention has been drawn to translationally restrained locations, such as fixed piers, for exterior girders as lateral bottom flange bending has become more prevalent. In conclusion, the findings from this investigation are not alarming; however, thermal loading may require further consideration in the future design of horizontally curved bridges that incorporate restrained supports with increasing degrees of curvature and skew.

REFERENCES

Abendroth, E. R., and L. F. Greimann. (2005). *Field Testing of Integral Abutments*. Iowa DOT Project HR-399. Ames, Iowa: Highway Division, Iowa Department of Transportation. CD-ROM.

American Institute of Steel Construction Inc. 2007. *Steel Construction Manual Thirteenth Edition*. United States: American Institute of Steel Construction, Inc.

Barr, P. J., N. Yanadori, M. W. Halling, and K. C. Womack. 2007. *Live-Load Analysis of a Curved I-Girder Bridge*. J. Bridge Eng. ASCE, 11(2), 160-168.

Doust, S. 2011. *Extending Integral Concepts to Curved Bridge Systems*. Ph.D. dissertation, University of Nebraska.

Dunker, K. 1985. *Strengthening of Simple Span Composite Bridges by Post-Tensioning.* Ph.D. dissertation. Iowa State University.

Hall, D. H., M. A. Grubb, and C. H. Yoo. 1999. *Improved Design Specifications for Horizontally Curved Steel Girder Highway Bridges*. NCHRP Report 424. Washington, DC: Transportation Research Board, National Research Council.

Hassiotis, S., Y. Khodair, E. Roman, and Y. Dehne. 2006. *Final Report Evaluation of Integral Abutments*. Hoboken, New Jersey Department of Transportation, Division of Research and Technology.

Kim, W. S., J. A. Laman, and D. G. Linzell. 2007. *Live Load Radial Moment Distribution for Horizontally Curved Bridges.* J. Bridge Eng. ASCE, 12(6), 727-736.

LaViolette, M. 2009. *Design and Construction of Curved Steel Girder Bridges*. Presentation.

Linzell, D., D. Hall, and D. White. 2004. *Historical Perspective on Horizontally Curved I Girder Bridge Design in the United States.* J. Bridge Eng. ASCE, 9(3), 218-229.

Lydzinski, J. and T. Baber. 2008. *Finite Element Analysis of the Wolf Creek Multispan Curved Girder Bridge*. Virginia Transportation Research Council, FHWA/VTRC 08-CR8. Charlottesville, Virginia.

Miller, J. and T. Baber. 2009. *Field Testing of the Wolf Creek Curved Girder Bridge: Part II: Strain Measurements.* Virginia Transportation Research Council, FHWA/ VTRC 09-CR14. Charlottesville, Virginia.

Mistry, Vasant C. *Integral Abutment and Jointless Bridges*. Conference of High Performance Steel Bridge. Baltimore, MD. Nov. 30-Dec. 1, 2000. 1-10. Retrieved from: http://www.nabro.unl.edu/articles/20002012/download/vasant.pdf. on May 2011.

Moorty, S., and C. W. Roeder. 1992. Temperature-Dependent Bridge Movements. *Journal of Structural Engineering* 118: 1090—105.

Nevling, D., D. Linzell, and J. Laman. 2006. *Examination of Level of Analysis Accuracy for Curved I-Girder Bridges through Comparisons to Field Data.* J. Bridge Eng. ASCE, 11(2), 160-168.

Offices of Bridges and Structures. 2011. *LRFD Bridge Design Manual*. Ames, IA. Iowa Department of Transportation.

Shryack, G., R. Abendroth, B. Phares, J. Ashlock, and L. Zachary. 2012. *Field Monitoring and Evaluation of Curved Girder Bridges with Integral Abutments*. Thesis, Iowa State University.

Thanasattayawibul, N. 2006. *Curved Integral Abutment Bridges*. Ph.D. dissertation, University of Maryland.

Tennessee Department of Transportation.1996. Highway Structures Design Handbook. Volume II, Chapter 5. Integral Abutments for Steel Bridges. U.S.A: American Iron and Steel Institute, National Steel Bridge Alliance.

Vasant, C. Mistry. *Integral Abutment and Jointless Bridges.* Washington, DC: Federal Highway Administration